1 **Dietary L-3,4-dihydroxyphenylalanine (L-DOPA) augments cuticular melanization in**
2 ***Anopheles* mosquitos while reducing their lifespan and malaria parasite burden**

3 Emma Camacho[1], Yuemei Dong[1], Christine Chrissian[2], Radames J.B. Cordero[1], Raúl G.
4 Saraiva[1], Yessenia Anglero-Rodriguez[1], Daniel F.Q. Smith[1], Ella Jacobs[1], Isabelle Hartshorn[1],
5 Jose Alberto Patiño-Medina[1], Michael DePasquale[1], Amanda Dziedzic[1], Anne Jedlicka[1], Barbara
6 Smith[1], Godfree Mlambo[1], Abhai Tripathi[1], Nichole A. Broderick[1], Ruth E. Stark[2], George
7 Dimopoulos[1], Arturo Casadevall*[1]

8 [1]Johns Hopkins University, Baltimore, USA

9 [2]City College of New York, New York, USA

10 Arturo Casadevall, Email: acasade1@jhu.edu

11 *Corresponding author

12

13 **ABSTRACT**

14 L-3,4-dihydroxyphenylalanine (L-DOPA), a naturally occurring tyrosine derivative, is prevalent in

15 environments that include mosquito habitats, potentially serving as part of their diet. Given its role

16 as a precursor for melanin synthesis we investigate the effect of dietary L-DOPA on mosquito

17 physiology and immunity to *Plasmodium falciparum* and *Cryptococcus neoformans* infection.

18 Dietary L-DOPA is incorporated into mosquito melanin via a non-canonical pathway and has a

19 profound transcriptional effect associated with enhanced immunity, increased pigmentation, and

20 reduced lifespan. Increased melanization results in an enhanced capacity to absorb

21 electromagnetic radiation that affects mosquito temperatures. Bacteria in the mosquito

22 microbiome act as sources of dopamine, a substrate for melanization. Our results illustrate how

23 an environmentally abundant amino acid analogue can affect mosquito physiology and suggest

24 its potential usefulness as an environmentally friendly vector control agent to reduce malaria

25 transmission, warranting further research and field studies.

26

27 **INTRODUCTION**

28 Malaria is a major public health threat exacerbated by the impact of climate change [1]. Global

29 warming has pushed mosquitoes to new latitudes and altitudes, prolonging the malaria

30 transmission season and increasing the risk to previously unaffected communities [2,3]. In addition,

31 human activities such as land development, intensive agricultural practices, and the widespread

32 use of chemical pesticides significantly influence the proliferation and spread of mosquito

33 populations [2]. As a result, the dynamics of disease transmission by these vectors are continually

1   evolving. A stark illustration of these public health consequences occurred last year when the

2   United States of America (USA) experienced nine cases of locally acquired malaria –marking the

3   first time in two decades that locally acquired transmission had occurred. Notably, eight of these

4   cases were reported in Florida and Texas, with an additional case identified in Maryland. This

5   alarming trend contrasts with the situation in 2003 when eight cases of locally acquired malaria

6   were identified and all were restricted to Florida's Palm Beach County. The *Anopheles* mosquito

7   vectors, responsible for transmitting malaria, are found throughout many regions of the US, posing

8   a substantial risk if they encounter a malaria-infected person [4]. In Africa, climate change is fueling

9   a perfect storm for malaria [3,5]. The combination of increased frequency of extreme weather events,

10   deforestation, warmer temperatures at higher altitudes, rapid spread of insecticide-resistant

11   *Anopheles* mosquitoes [6], and emergence of urban mosquito vectors like *Anopheles stephensi* [7]

12   threaten progress in malaria control and pose greater risks to human health.

13   Most vector borne diseases have been mitigated through the implementation of efficacious vector

14   control programs [8]. However, maintaining the long-term sustainability of such programs is difficult

15   and often impractical. In the case of malaria, prior to the use of insecticides, vector control

16   strategies relied on understanding the ecology of local vectors such as changing the aquatic

17   habitats where the vector developed (e.g., draining swamps, applying oil to open water bodies,

18   cutting vegetation at edges of ponds/streams). These interventions were highly successful but

19   labor intensive and they had huge negative environmental impact [9]. Consequently, environmental

20   management practices were replaced by insecticide-based vector control. Despite initial success

21   – between 2000 to 2015, the employment of nets impregnated with residual insecticides led to a

22   reduction in over 50% of malaria cases in Africa – these efforts were compromised by the

23   emergence of insecticide-resistance in the mosquito vectors and drug-resistance in the malaria-

24   carrying parasites which they harbor [10,11].

25   Considering the challenges outlined above, the World Health Organization (WHO) has urged the

26   development of cost-effective, sustainable, and environmentally safe vector-control interventions.

27   As adult mosquitoes of both sexes, including hematophagous species, feed from floral nectar as

28   a common nutritional source [12], attractive toxic sugar baits (ATSBs) are alternative and potential

29   new tools [13]. These mosquito control methods rely on appealing cues and sugar loaded with

30   distinct agents such as transgenic entomopathogenic fungi [14], genetically modified bacteria (para-

31   transgenesis) that confer mosquito refractoriness [15], or natural microbiota that result in increased

32   resistance and/or decreased fitness [16].

2

1 In insects, melanin plays an essential role in three physiological processes: cuticular melanization,

2 wound healing, and immunity [17]. Research on the complex nature of plant-insect interactions has

3 shown that insects adapt to L-DOPA-rich diets [18-20]. For instance, the pea aphid *Acyrthosiphon*

4 *pisum* uses plant-derived L-DOPA to promote melanin synthesis for wound healing and UV

5 protection while sequestering high toxic compound levels [18]. Consequently, we aim to investigate

6 the potential of 3,4-dihydroxyphenylalanine (L-DOPA), a melanin precursor found naturally in

7 flowers of the faba bean, *Vicia faba* L. (Fabaceae) [21,22]. Extrafloral nectaries of these legumes

8 also emit headspace volatiles like linalool, known to attract *Culex*, *Aedes* and *Anopheles*

9 mosquitoes [23,24]. We hypothesize that adult *A. gambiae* mosquitoes modulate melanin-related

10 physiological processes in response to a sugar diet supplemented with L-DOPA, thereby reducing

11 their olfactory susceptibility to foreign organisms that could pose a threat to humans.

12 Consequently, we assess the oral toxicity of L-DOPA concentrations in a sugar solution, define

13 the transcriptional profile of *A. gambiae* female mosquitoes in response to dietary L-DOPA and

14 evaluate its functional impact on key vector life traits (Fig. 1). L-DOPA-fed *A. gambiae* female

15 mosquitoes exhibit downregulation of essential immune-related genes, have reduced malaria

16 parasite and fungal burden, enhanced cuticular melanization, shortened life span, and suppress

17 expression of critical genes involved in the synthesis of cuticular hydrocarbons. Our findings

18 suggest a potential role for L-DOPA in malaria control strategies that target mosquito

19 reproduction.

20

21 **RESULTS**

22 **Effects of dietary L-DOPA on survival of *A. gambiae* female mosquitoes.**

23 *A. gambiae* females rely mainly on a blood meal to obtain phenylalanine as the initial substrate

24 for the melanization process. In contrast, male mosquitoes depend exclusively on plant sources

25 (Fig. 2). To investigate whether a sugar solution supplemented with L-DOPA had a beneficial or

26 detrimental impact on melanin-related physiological processes of adult mosquitoes, we first

27 assessed its effect as a supplement to sugar meals on longevity, as a measure of mosquito

28 fitness. We provided 3–4-day-old female mosquitoes with a low sugar solution supplemented with

29 L-DOPA at concentrations ranging from 0.2 to 10 mM (0.4 to 20% w/w) and then monitored their

30 survival over a 14-d period. These L-DOPA concentrations were comparable to those reported in

31 natural sources, which range from 0.2 to 7.7% (w/w) [21,25-30]. We observed that after 8 d of L-

32 DOPA exposure, mosquitoes fed on L-DOPA solutions at most concentrations started to

33 experience a drastic increase in mortality, except for those fed on 1 mM (2%) L-DOPA, whose

1 survival exceeded that of the control (Fig. 3a). By 14 d, mosquitoes fed with L-DOPA solutions at

2 concentrations lower than 1 mM exhibited a mortality of ~50%, while at higher doses mortality

3 increased in a dose-response relationship. Notably, analysis of the accumulative survival at

4 different time points revealed that dietary L-DOPA exhibited a clear biphasic dose-response (Fig.

5 3b). Conversely, when providing dopamine in the sugar meal the hormesis effect disappeared,

6 with control mosquitoes and those fed with up to 1 mM dopamine-sugar dying at an equal pace

7 (Figs. 3c, 3d). Consequently, we used 1 mM L-DOPA in subsequent experiments.

8

9 **Dietary L-DOPA affects expression of mosquito immune- and cuticle-related genes.**

10 To identify genes whose expression was affected by a non-toxic concentration of L-DOPA, we

11 collected female *A. gambiae* mosquitoes post 1 mM L-DOPA feeding of the sugar meal during 4

12 d and performed RNA sequencing (mRNA-seq) on whole mosquitoes (headless) and midguts.

13 We observed 902 and 165 differentially expressed genes between L-DOPA-fed versus sucrose-

14 fed controls (≥ 2-fold change, $P < 0.05$) in the whole mosquitoes and midgut samples, respectively

15 (Fig. 4). In whole mosquitoes, these included 808 downregulated and 94 upregulated genes, both

16 overrepresented in the functional category of stress-related (R/S/M; oxidoreductive, stress-

17 related, mitochondrial) (Figs. 4a, 4b). In midguts, we observed 50 downregulated and 115

18 upregulated genes. Downregulated genes were overrepresented in the functional categories of

19 transport, DNA-related (R/T/T; replication, transcription, translation), and stress-related (Figs. 4c,

20 4d, Supplementary Data 1, Supplementary Fig. 1). Unexpectedly, key genes involved in the

21 melanin biosynthesis pathway such as prophenoloxidase 5 (PPO5) (AGAP012616) and

22 dopachrome-conversion enzyme (DCE) (AGAP005959) were significantly downregulated.

23 Diverse immune-related gene families involved in pattern recognition receptors (PRRs) (e.g.,

24 *peptidoglycan recognition proteins* (PGRP), *scavenger receptor* (SCR), and *galectins* (GALE)),

25 signal modulation and amplification (e.g., *clip domain serine proteases* (CLIP) and *serpins*

26 (SRPN)), signal transduction pathways (e.g., TOLL), and other effector systems (e.g., *caspases*

27 (CASP) also exhibited significant downregulation. Furthermore, two critical genes for dopamine

28 metabolism in insects, dopamine beta-monooxygenase (DBH) (AGAP010485) and dopa

29 decarboxylase (DDC) (AGAP009091), which participate in the synthesis of octopamine (main

30 neurotransmitter) and cuticle, respectively, were also downregulated. By contrast, the immune-

31 related dally protein (AGAP005799) involved in signal transduction was significantly upregulated

32 (Fig. 5a, upper panel, Supplementary Data 1). In the midguts, the most significantly upregulated

33 gene corresponded to phosphoinositide-3-kinase, regulatory subunit (PI3K) (AGAP005583) that

participates in bacterial phagocytosis and apoptosis, and autophagy in *Drosophila*[31] (Fig. 5a, lower panel; Supplementary Data 1).

Regarding cuticle-related genes, transcriptional profiles of whole mosquitoes showed that L-DOPA-supplementation was associated with an extensive downregulation of gene families involved in cuticle regulation, metabolic detoxification, and synthesis of cuticular hydrocarbons. These included: cuticular proteins (e.g., AGAP000820 and AGAP000986); chitinase (CHT5-5, AGAP013120); chitin synthase 1 (CHS1A, AGAP001748); cytochrome P450s; propionyl-CoA-synthase (AGAP001473); and elongases (AGAP005511, AGAP005512, AGAP013219). Notably, upregulated genes in L-DOPA-fed mosquitoes corresponded to hexosaminidase D (AGAP004270) and glutathione S-transferase epsilon class 6 (GSTE6) (AGAP009191) (Fig. 5b, upper panel, Supplementary Data 1). The latter gene is associated with the development of insecticide resistance in the malaria vector *Anopheles funestus* [32]. Similarly, in the midgut, cytochrome P450s and chitin-related genes were downregulated while *Jheh2*, a gene coding for juvenile hormone epoxide hydrolase, was upregulated (Fig. 5b, upper panel, Supplementary Data 1).

Notably, almost a third (255 out of 902) of the genes differentially regulated in response to L-DOPA corresponded to hemocyte-associated genes. Most of these were oenocytoid-related (76.9%) versus granulocyte-related immune cell subtypes (19.2%), as defined by scRNA-seq hemocytes clustering performed by Kwon *et al* [33]. These genes are involved in multiple functional categories including immunity, lipid metabolism, proteolysis, transport, and chemosensory systems such as odorant binding proteins (OBPs) and G-coupled protein receptors (GPCRs) (Supplementary Data 1). Collectively, our transcriptional analysis suggests that dietary L-DOPA was associated with a global modulation of genes beyond those related to melanin-associated processes.

Dietary L-DOPA promotes mosquito resistance to malaria parasite and fungal infection.

To investigate whether a L-DOPA-supplemented sugar meal could modulate *P. falciparum* infection in *A. gambiae* mosquitoes, we fed *Anopheles* female mosquitoes on L-DOPA containing solutions (0.2 mM, 0.6 mM, and 1 mM) for 4 d prior to *P. falciparum* infection. The intensity of the parasite infection was assessed by enumeration of *P. falciparum* oocysts at 8 d post-infection (dpi). Mosquitoes fed with a sugar meal supplemented with L-DOPA demonstrated a dose-dependent reduction of the *P. falciparum* parasite burden with a significant reduction for the 1 mM

L-DOPA in comparison to the sugar-fed control (median number of oocysts 2 vs 5, *p*= 0.0081). L-DOPA supplementation also reduced the infection prevalence (77.5% vs 87.3% at 1 mM in comparison to the control) (Fig. 6a, left panel). Using dopamine instead of L-DOPA in the sugar meal was also associated with a significant reduction of *P. falciparum* infection burden in a dose-dependent manner relative to the sugar-fed controls. At the highest dose, 1 mM dopamine, the median number of oocysts was 2 vs 7, *p*=0.0019 in comparison to the control, and the prevalence of infection was also reduced (81.1% vs 87.5%) but to a lesser degree than in the presence of an L-DOPA-supplemented sugar meal (Fig. 6a, right panel). No melanized parasites were observed in these experiments at either 2 or 8 dpi, regardless of whether L-DOPA- or dopamine-supplemented sugar meals were provided following parasite infection (data not shown), indicating that the reduction in parasite infection was due to a non-melanin-based immune response. Given that nectars provide mosquitoes with L-DOPA, we investigated whether L-DOPA directly exhibits *in vitro* antiplasmodial activity to both sexual and asexual stages of the human malaria parasite. At 1 mM L-DOPA, sexual stages of *P. falciparum* exhibited significant toxicity (32.4% survival vs sugar-fed control, *p* < 0.0001), while the viability of asexual stages of the parasite was nearly abolished at 1 mM L-DOPA and drastically reduced at 0.5 mM L-DOPA (26.3% survival vs control) (Fig. 6b).

A. gambiae triggers a melanin-based immune response against fungi [34,35]. To ascertain whether L-DOPA supplementation promoted fungal melanization, we challenged mosquitoes with an intrathoracic injection of *Cryptococcus neoformans* (H99-GFP strain), prior to L-DOPA exposure for 4 d. Fungal viability was assessed by measuring the number of fungal colony-forming units (CFUs) 24 h after injection and by monitoring H99-GFP fluorescence, a previously validated reporter strain for assessing fungal viability[36]. L-DOPA-fed mosquitoes showed reduced number of fungal CFUs in comparison to the control (Fig. 6c) and revealed efficiently melanized yeast cells (Fig. 6d). Furthermore, we found that despite downregulation of dopa decarboxylase (DDC), a key gene on the melanization pathway, other genes involved in *Plasmodium* parasite killing and survival —specifically the antimicrobial peptide gambicin (GAM)[37] and the leucine-rich immunomodulator 15 (LRIM15)[38]— were significantly deregulated, affecting *Plasmodium* parasite development (Fig. 6e). Our analyses demonstrated that, despite significant downregulation of canonical melanization-related genes that was validated by qRT-PCR (Supplementary Fig. 2), L-DOPA-supplementation promoted both antiplasmodial and anti-fungal response in *A. gambiae* female mosquitoes.

1 **Dietary L-DOPA enhances mosquito cuticular melanization.**

2 The insect cuticle protects against physical trauma (rigid cuticle) and flexibility to support joint

3 areas allowing mobility (soft cuticle) [39]. Melanin is primarily thought to be involved in the formation

4 of rigid cuticles, though its participation in the biogenesis of flexible cuticles is uncertain. While

5 assessing daily mortality, we serendipitously noticed that the 1 mM L-DOPA-fed mosquitoes

6 displayed a greater darkening of the cuticle pigmentation in comparison to sucrose-fed controls

7 (Fig. 7a, upper panel). Thus, we explored the contribution of dietary L-DOPA to insect cuticular

8 melanization by allowing *A. gambiae* female mosquitoes to feed with a sugar solution

9 supplemented with L-DOPA (0.2 mM to 1 mM) for up to 14 d. At 8 and 14 d, we observed and

10 measured a dose-dependent darkening of the mosquito cuticle; 1 mM L-DOPA-fed mosquitoes

11 exhibited significantly darker pigmentation relative to sugar-fed control mosquitoes (Fig. 7a, lower

12 panel)**.** To further assess the mosquito cuticular ultrastructure and chemical nature of its pigment,

13 we used transmission electron microscopy (TEM) to examine the cuticular architecture of legs

14 from *A. gambiae* female mosquitoes after 8 d of exposure to the L-DOPA diet. Micrographs from

15 female L-DOPA-fed mosquitoes revealed a distinct microstructure of the leg endocuticle layer in

16 comparison to the sucrose-fed control (Fig. 7b, top panel). The mean thickness of the total cuticle

17 was significantly greater (mean = 2,424.11 ± 467.97 nm) than that of the control (mean = 1,962.63

18 ± 302.91 nm) **(**Fig. 7b, bottom panel). In response to the L-DOPA diet, female mosquitoes showed

19 cuticle enrichment promoted by an increase of both procuticle layers (endocuticle and exocuticle).

20 In addition, we determined the accumulation of melanin in whole mosquitos using solid-state NMR

21 with ^{13}C-isotopically-labeled L-DOPA. Adult female *A. gambiae* mosquitoes were fed with 1 mM

22 ring-^{13}C-L-DOPA in sucrose for 8 d to augment the ssNMR signal intensity. To estimate the

23 relative amounts of long-chain lipids, polysaccharides, and melanin in *A. gambiae* mosquitoes fed

24 with or without labeled L-DOPA, we acquired quantitatively reliable ^{13}C direct-polarization magic-

25 angle spinning (DPMAS) NMR data. In comparison to the control, spectra from ring-^{13}C-L-DOPA-

26 fed female mosquitoes displayed increased signal intensities at 110-160 ppm which are

27 characteristic of the indole-based melanin pigment (Fig. 7c, green arrows in left panel), suggesting

28 that mosquitoes used ring-^{13}C-L-DOPA to synthesize cuticular melanin. To determine whether

29 mosquitoes broke down ring-^{13}C-L-DOPA for nutritional purposes, we also acquired ^{13}C cross-

30 polarization magic-angle spinning (CPMAS) spectra that favored the most rigid constituents. This

31 latter study corroborated the nearly exclusive use of ring-^{13}C-L-DOPA for pigment production:

32 signals corresponding to polysaccharides (~55-105 ppm) as well as those corresponding to

33 aliphatic carbons (10-40 ppm) were largely unchanged in integrated intensity upon feeding with

34 ring-^{13}C-L-DOPA (Fig. 7c, right panel). Interestingly, L-DOPA supplementation also increased the

1   content of indole groups but reduced the cuticular thickness of legs in male *A. gambiae*

2   mosquitoes (Supplementary Fig. 3). These mosquitoes also displayed a modest increase in their

3   chitin content (0.64 ± 0.07 nmoles of glucosamine per mg of whole mosquito dry weight) in

4   comparison to the sucrose-fed controls (0.46 ± 0.06 nmoles of glucosamine per mg of whole

5   mosquito dry weight) (Fig. 7d). Furthermore, we tested whether the augmented indole-pigment

6   content corresponded to melanin by performing electron paramagnetic resonance (EPR)

7   measurements. EPR is a particularly effective methodology that detects a remarkable

8   characteristic feature of this biopolymer, the presence of a population of stable organic free

9   radicals [40]. Analysis of the acid-resistant material isolated from L-DOPA-fed mosquitoes revealed

10   a spin concentration that decreased to 0.81-fold of its value (14.55 vs 17.75, scaled by mass)

11   compared with sugar-fed controls (Fig. 7e). Lastly, we demonstrated that melanin synthesis was

12   not driven by DCE providing a L-DOPA diet to the *Aedes aegypti* yellow (DCE2, AAEL006830)

13   mutant strain[41], which is defective for eumelanin synthesis. This mutant mosquito strain also

14   exhibited a spin concentration that diminished to 0.3-fold of its value (2.36 vs 7.60) compared with

15   its sugar-fed control. The lower spin concentrations of L-DOPA supplemented samples in

16   comparison to controls is suggestive of an enhanced radical scavenging activity— a key melanin

17   property[42]. Notably, the high spin concentration exhibited by the *A. gambiae* L-DOPA

18   supplemented samples compared with the *Aedes* L-DOPA-fed mutant mosquito strain (14.55 vs

19   2.36, respectively) could imply the isolation of different types of melanins (a mixture of

20   pheomelanin/eumelanin vs eumelanin) with distinct antioxidant properties. These results agree

21   with our fungal eumelanin sample, used a control, which displayed a spin concentration of 4.26.

22   Further studies will be required to gain a deeper understanding of this system.

23   In sum, oral L-DOPA promoted mosquito cuticle melanization via a non-canonical pathway

24   independent of L-DOPA conversion into dopachrome, impacting the thickness of both endocuticle

25   and exocuticle layers.

26

27   **Enhanced cuticle melanization fails to promote insecticide resistance yet raises mosquito**

28   **body temperature and reduces lifespan.**

29   Previous studies in *Anopheles* mosquitoes have shown that changes in the cuticle structure are

30   associated with insecticide-resistance [43,44]. Thus, we set out to determine whether enhanced

31   cuticular melanization impacted female *A. gambiae* resistance to pyrethroids, the only WHO-

32   approved insecticide used on long-lasting insecticide-treated nets (LLINs). Using WHO-approved

1   papers impregnated with 0.05% deltamethrin for 1 h exposure, L-DOPA-fed *A. gambiae* female

2   mosquitoes demonstrated susceptibility to pyrethroids (98.7± 3.3% mortality rate in 24 h). Despite

3   their highly melanized and thicker legs, L-DOPA-fed *A. gambiae* female mosquitoes were

4   susceptible to 0.05% deltamethrin.

5   Dark pigmentation is associated with enhanced ability to capture heat from electromagnetic

6   radiation on animals, plants, and fungi [45]. In insects, melanization (melanism) is associated with

7   negative or positive consequences in thermal adaptation, mating, cuticle strength, etc. that impact

8   their fitness and ecology [46-48]. To probe mosquitoes' thermal response to visible electromagnetic

9   radiation, we used a thermal camera to measure the maximum average body temperature of L-

10   DOPA-fed individual mosquitoes after being exposed to a white light mimicking sunlight. Female

11   *A. gambiae* mosquitoes fed with L-DOPA for 8 d maintained an apparent average body

12   temperature that was 0.5 – 2.0 °C higher that sugar-fed control mosquitoes, following 1 min of

13   irradiation (Fig. 8a, Supplementary Fig. 4). Notably, 1 mM L-DOPA-fed mosquitoes were

14   significantly warmer than control. These mosquitoes exhibited the highest temperature, both pre-

15   and post-irradiation (Fig. 8b, Supplementary Fig. 4). Because trade-offs between heat tolerance

16   and life-history are observed in insects [49], we further investigated whether longevity of L-DOPA-

17   fed mosquitoes differed from those of controls. We measured the longevity of female mosquitoes

18   when maintained on the L-DOPA diet (Fig. 8c). The lifespan of female mosquitoes was

19   significantly decreased when maintained on a sucrose meal supplemented with 1 mM L-DOPA

20   (Wilcoxon test, Chi-square, 13.74, p = 0.0002). These mosquitoes exhibited no apparent changes

21   in reproductive fitness: number of eggs laid (Fig. 8d) and hatching rate (Fig. 8e).

22

23   The mosquito microbiome includes bacteria that produce dopamine.

24   Unlike mammalian tyrosinases, which utilize L-DOPA as a melanin precursor [50], insect

25   phenoloxidases preferentially use dopamine over L-DOPA [51]. This led us to investigate how

26   dietary L-DOPA was metabolized in female mosquitoes and whether the mosquito microbiome

27   harbors dopamine-synthesizing bacteria. Contrary to findings in *Aedes albopictus* [52], we observed

28   the intriguing trend whereby as L-DOPA levels increased in the sugar meal, dopamine levels in

29   mosquitoes decreased (Fig. 9a). Leveraging our experience with studying fungal melanization in

30   *Cryptococcus* spp., which can be triggered by dopamine synthesized by bacteria [53], we explored

31   whether gut microbiota isolated from field-caught mosquitoes have the potential to serve as an

32   endogenous source of dopamine. *Cryptococcus* spp., known to be members of the mosquito gut

9

mycobiome [54,55], depend exclusively on exogenous precursors for melanin synthesis (e.g., L-DOPA, dopamine, epinephrine, and norepinephrine) [56]. We selected thirteen bacterial strains that had been previously isolated from the midgut of field-caught *Anopheles* [16] and *Aedes* [57] mosquitoes plus a strain isolated from the soil[58,59] (Supplementary Table 1) and conducted a plate confrontational assay whereby bacteria that produce dopamine trigger melanization in *Cryptococcus neoformans* [53]. After eye inspection of the plates, we noticed that five bacterial isolates consistently induced melanization (brown pigmentation) in both of our positive control strains (*C. gattii* WM179 and *C. neoformans* H99), at both room temperature and 30°C. As expected, no pigmentation was observed in the *C. neoformans* LAC1 mutant strain (negative control), in which melanin synthesis is compromised by the deletion of its laccase gene (Fig. 9b). The melanin-inducing bacteria were identified as: *Comamonas* sp., *Enterobacter hormaechei*, *Aeromonas hydrophila*, *Serratia marcescens*, and *Chromobacterium subtsugae* ΔvioS (ΔvioS). To verify the chemical nature of the soluble compound released by mosquito-derived bacteria that promoted cryptococcal melanization, we used a Fast Protein Liquid Chromatography (FPLC) protocol for recovering dopamine from bacterial supernatants grown in Luria-Bertani (LB) media for up to 96 h at 30°C. The chromatograms displayed a peak between 4.39 and 5.66 min matching the position of the dopamine spike peak. We observed that peaks varied depending on the bacterial species and tended to be larger as the incubation time increased (Supplementary Fig. 5). Therefore, we collected peaks at 96 h of culture incubation, removed cells by quick centrifugation, filter-sterilized the supernatants, acidified them to pH 4.0 with 1 M HCl to maintain dopamine stability, and kept them on ice, and away from light. Samples were further identified as dopamine and quantified by Electrospray Ionization (ESI) Mass Spectrometry (MS). Dopamine production was verified from four strains at concentrations ranging from 7 ng/ml to 67.5 ng/ml. These were the dopaminergic bacteria identified (concentration of dopamine detected): *Aeromonas hydrophila* (7.10 ± 0.4 ng/ml), *Comamonas sp.* (7.00 ± 0.1 ng/ml) and *Enterobacter hormaechei* (67.5 ± 2.4 ng/ml). No dopamine was quantified for *Serratia marcescens* under the tested conditions. The limit of quantification of the ESI MS was 2.5 ng/ml.

Discussion

In insects, melanin is synthesized both in the exoskeleton (cuticle) and inside the body, including by the immune system, which uses melanization as an antimicrobial mechanism [60-62]. The cuticle is crucial for insect survival, making it a primary target for pest and disease vector control. Its mechanical properties (i.e., rigidity and flexibility) are related to various chitins, proteins, and the type and abundance of sclerotization or protein crosslinking occurring within [63]. This study

1   demonstrates that *Anopheles* mosquitoes can use dietary L-DOPA to enhance cuticle

2   melanization, leading to increased body pigmentation, cuticular thickness in the legs, overall

3   indole and chitin content, and a key EPR signal (Fig. 7). Given the abundance of L-DOPA in the

4   environment and the potential microbiome sources of dopamine, our results have important

5   implications for mosquito biology and potential control strategies.

6   Cuticular melanogenesis is closely related to cuticular hardening or sclerotization. Both are

7   oxidative processes occurring in the same tissues and use L-DOPA or dopamine as precursors;

8   however, the participation of laccase 2 (AGAP008731) and dopamine derivatives such as *N*-

9   acetyl-dopamine (NADA) and *N*-β-alanyldopamine (NBAD) in mediating covalent crosslinks

10 between cuticular proteins and/or between cuticular proteins and chitin fibers is exclusive to the

11 sclerotization process [17,51]. Our data demonstrate that mosquitoes can metabolize L-DOPA via a

12 non-canonical pathway using 3,4-dihydroxylphenylacetaldehyde (DOPAL) synthase (Fig. 10a).

13 As a detoxification mechanism, L-DOPA is directly converted into DOPAL and hydrogen peroxide.

14 The resulting hydrogen peroxide further oxidizes the DOPAL catechol ring, leading to the

15 formation of a melanized and flexible cuticle crosslinked with cuticular proteins, while bypassing

16 the conversion of L-DOPA to dopamine [63,64]. The buildup of DOPAL promotes oligomerization and

17 the formation of quinone adduct ("quinonization"), which inhibits its own metabolism and the

18 activity of other enzymes involved in the melanin biosynthesis [65]. Therefore, this study supports

19 that L-DOPA-induced downregulation of key melanization pathway genes (e.g., *DDC* and *DCE*)

20 occurs at transcriptional level leading to a reduction of their protein translation/production (Fig.

21 10b). Further studies are required to demonstrate DOPAL buildup and protein modification.

22 Dietary L-DOPA affects multiple mosquito physiological pathways in a dose-dependent manner

23 (Figs. 3, 6, 7, 8, 9). The strong allelopathic activity of L-DOPA may explain our observations [27],

24 Depending on the cellular redox potential, L-DOPA behaves as a prooxidant (at alkaline pH)

25 promoting oxidative damage and covalent modification of proteins, or as an antioxidant (at acid

26 and neutral pH) scavenging initiating radicals by electrostatic interactions and chelating metal

27 ions to prevent their participation in radical formation [66]. Our analyses demonstrate that L-DOPA-

28 supplemented sucrose meals induced a biphasic dose-response (Fig. 3b), a phenomenon

29 known as hormesis. Hormesis occurs in response to moderate environmental or self-imposed

30 challenges, which causes a system to improve its functionality and/or tolerance when faced with

31 more severe challenges [67,68]. This phenomenon is widespread in nature and has been reported

32 for various molecules, including nitric oxide, prostaglandins, dopamine, and other molecules[69].

33 Hormetic-like responses involve the simultaneous stimulation of many independent cellular

1   functions/endpoints and define the boundaries of biological plasticity [68].

2

3   Despite marked downregulation of immune-related genes (Fig. 5a), oral L-DOPA promoted
4   antimicrobial activity in *A. gambiae* female mosquitoes (Fig. 6). Our *in vitro* analyses show that L-
5   DOPA concentrations above 0.5 mM impair *P. falciparum* development at both sexual and
6   asexual stages. This aligns with a previous finding that L-DOPA induces apoptosis in *P. berghei*
7   ookinetes under similar conditions [70]. Conversely, given the particularity of our L-DOPA diet (an
8   amino acid analog within a low sucrose concentration) and the complexity of the mosquito
9   digestion system (sugar and protein meals have distinct compartmentalization) [71], the enhanced
10 resistance to parasite burden exhibited by L-DOPA-fed mosquitoes might reflect multifactorial
11 mechanisms. At least two possible scenarios, non-mutually exclusive, could explain the results.
12 First, L-DOPA-mediated acidification of midgut pH could block parasite development at the midgut
13 lumen thus reducing midgut invasion [72]; mean pH measurements of 1 mM L-DOPA-sugar solution
14 dropped from 8.3 to 6.7 within 72 h (Supplementary Fig. 6). Second, the restrictive sugar diet
15 (1.5% sucrose) may trigger a metabolic switch that functionally primes the mosquito to resist
16 pathogen invasion [73]. In line with the latter scenario, the upregulation of the Dally protein
17 (AGAP005799), phosphoinositide-3-kinase (PI3K) (AGAP005583), and juvenile hormone (JH)
18 (AGAP008685) could reflect an integrative response from the insulin/TOR signal transduction
19 pathway, sensing not only nutritional information but also other environmental cues such as
20 temperature and foreign organisms to fine-tune allocation of resources and promote fitness [74-77].

21 In most insects, genes encoding enzymes involved in melanization and sclerotization are referred
22 to as pleotropic [78-80], supporting the hypothesis that pleiotropy (i.e., expression of multiple traits
23 by a single gene) drives the coevolution of correlated traits [81]. Such is the case for cuticle
24 pigmentation, which was significantly darkened in 1 mM L-DOPA-fed mosquitoes (Fig. 7). Its
25 association with increased thickness in female mosquitoes immediately raises a concern for
26 insecticide resistance given that several studies in disease vectors have reported this linkage [43,82-
27 84]. Other mechanisms extensively shown to be involved in resistance to insecticides are alteration
28 of target molecule, reduced cuticle permeability, and metabolic clearance via overexpression of
29 detoxification protein families such as cytochrome P450 (CYPs), glutathione S transferases
30 (GSTs), and esterases [85]. In agreement with *A. gambiae* susceptibility to deltamethrin upon L-
31 DOPA feeding, these mosquitoes exhibit a drastic downregulation of GSTs, carboxylesterases,
32 cuticular proteins, and CYPs including CYP4C27 (AGAP009246), which were previously
33 associated with insecticide resistance in *A. gambiae* [86] (Fig. 5b, Supplementary Fig. 2). It is worth
34 mentioning that the slight increase of chitin content measured in whole L-DOPA fed mosquitoes

corresponds to a mixture of chitin and chitosan, given that the samples were deacetylated before performing the colorimetric reaction. Regardless of the chemical processing, based on our previous work with melanized cryptococcal cell walls [42,87], as well as the observed downregulation of chitin synthase 1 (CHS1A,B) (AGAP001748), we propose that dietary L-DOPA induces an increase of chitosan within the mosquitoes legs. This, in turn, promotes melanin deposition and thus translates into augmented cuticular pigmentation. As predicted by the thermal melanism hypothesis [88], increased mosquito pigmentation was associated with augmented heat absorption for the 1 mM L-DOPA fed mosquitoes (Figs. 8a-b) supporting an adaptative trait also described in insects from various orders [89-91]. *Anopheles* mosquitoes are poikilotherms, so ambient temperature strongly influences developmental processes, behaviors, and even survival [92]. These effects in thermoregulation could have an ecological impact; indeed, darker mosquitoes displayed a reduced longevity (Fig. 8c). This negative effect could be attributable to low tolerance to heat associated with starvation[49] given that our polyphenol-rich diet (e.g., dietary L-DOPA) with low sucrose concentration mimics calorie restriction [93]. Another possible explanation for the decreased life span is that dietary L-DOPA might be affecting *A. gambiae* cuticular hydrocarbon composition (CHC), therefore increasing susceptibility to desiccation. This reasoning is based on our RNA-seq data from L-DOPA-fed *A. gambiae* female mosquitoes, which reveals a strong downregulation of genes involved in CHC synthesis, including three genes specifically enriched in *A. gambiae* oenocytes (immune cells associated to melanin production) (Figure 5B). One of these genes, AGAP001473 [3.05-fold change, p = 0.0004 compared to sugar-fed controls, validated by qRT-PCR (Supplementary Fig. 2), encodes a single propionyl-CoA synthetase responsible for synthesizing methyl-branched hydrocarbons (mbCHCs) [94]. These mbCHCs have melting points (temperature at which these hydrocarbons transition from a solid to a liquid state) above ambient temperature, meaning they likely play a role in both reducing water loss and mediating chemical communication [95]. We hypothesize that in response to dietary L-DOPA, *A. gambiae* female mosquitoes exhibit a distinct CHCs profile, skewed toward short-chain (<25C) and non-branched CHCs, leading to increased susceptibility to desiccation. Further experimental testing will be required to test this hypothesis.

Concomitant with dietary L-DOPA, our evidence that gut microbiota colonizing adult *Aedes* and *Anopheles* mosquitoes can synthesize dopamine (Fig. 9b) strongly suggests that the mosquito gut microbiome could also play a role in the effects reported here. Indeed, certain *Enterococcus* and *Bifidobacterium* species identified in in the gut of Parkinson's Disease patients can metabolize L-DOPA into dopamine or other metabolites like 3,4-dihydroxyphenyl pyruvic acid (DHPAA) [96,97]. The mosquito microbiome is a critical modulator of vector competence and vectorial capacity,

also influenced by the mosquito diet [16,98,99]. The interactions between fungal and bacterial microbes shape fungal microbiome communities within the mosquito gut, which are dominated by Ascomycota and Basidiomycota. Among these are *Candida* and *Cryptococcus* spp.[54,55] which can use catechols (L-DOPA and dopamine) as substrates for melanin synthesis [56]. Therefore, as previously reported by other authors [100-102], midgut microbiota could also contribute to mosquito homeostasis by detoxifying toxic compounds that modulate symbiotic relationships between the gut microbiome and their host. In this line of thinking, the L-DOPA-modulated microbiome can also promote a certain pH at the midgut, thus favoring either prooxidant or antioxidant properties of L-DOPA [72]. Interestingly, recent research in *Aedes aegypti* demonstrated that higher levels of juvenile hormone (JH) in mated and virgin-JH treated in comparison to virgin mosquitoes promoted establishment of the midgut microbiota, midgut enlargement and allocation of energetic resources to enhance fecundity while inducing some immunosuppression. L-DOPA-fed female mosquitoes had no defects in reproduction (Figs. 8d-e). Recent evidence in the invertebrate model *Daphnia magna* showed that its gut microbiome is responsible for the synthesis of L-DOPA, which may serve as a signaling molecule modulating host-microbiome interactions relevant for key life traits [103]. The existence of a gut-to-brain signaling axis modulated by 5-hydroxytryptamine innervations in the midgut tissue of *Anopheles stephensi* mosquitoes was also recently suggested [104]. In addition, the contribution from hemocytes as key regulators of mosquito immunity cannot be ruled out. In *Drosophila*, hematopoietic progenitors can directly sense and respond to systemic (sugar/insulin) and nutritional (amino acids) signals via coordinated communication between organs [105].

Furthermore, insect herbivores can use plant-synthesized compounds by ingesting and storing them in their hemolymph, integument (cuticle), and other compartments such as cuticular cavities, in subcuticular compartments, fat body, or in exocrine defense glands [106]. This process, known as chemical sequestration, requires the active transport of the compound from the gut lumen across the midgut epithelium and to other compartments via ATP-binding cassette (ABC) and solute carrier (SLC) transporters [107]. Unlike metabolic resistance, which involves alteration and detoxification of the compound or plant toxin, sequestered compounds must preserve their pharmacological activity, allowing insects to benefit from them. For instance, sequestered aromatic compounds have been linked to defense, reproduction, or exoskeleton stabilization in various insect orders, including Diptera[108]. Our RNA-seq data from midguts of L-DOPA-fed mosquitoes reveals upregulation of AGAP006221, a gene coding for an aldehyde oxidase, as well as two transport-related genes—sodium-dependent nutrient amino acid transporter 5 (AGAP010857) and nicotinic acetylcholine receptor subunit alpha 2 (AGAP002972).

1   AGAP006221 is highly upregulated in *A. stephensi* at early stages (up to 24 h) post permethrin

2   exposure, thereby playing a critical role in its detoxification process[109]. Interestingly, in response

3   to the insecticide-mediated stress, these authors found a broad downregulation of CYPs, GSTs,

4   and carboxylesterases suggestive of reallocation of energetic resources during insecticide stress,

5   as we also demonstrated in *A. gambiae* post dietary L-DOPA exposure. Given the pleotropic

6   effects of dietary L-DOPA in *Anopheles* mosquitoes' biology, supported by its strong

7   allelochemical activity and potential direct role as a neurotransmitter mediating host-gut

8   microbiome interactions [103], it was out of the scope of this work to elucidate the mechanism(s)

9   responsible for the reduction of dopamine levels in whole mosquitoes as L-DOPA concentrations

10   in the sugar increased (Fig. 9a). However, in agreement with our findings, L-DOPA sequestration

11   with the same dopamine trend has also been observed in the pea aphid (*A. pisum*) when feeding

12   on an L-DOPA-rich plant, the broad bean (*V. faba*). This phenomenon enhances wound healing

13   and confers UVA-radiation protection to the pea aphid [18]. A potential explanation for this could

14   involve a gut symbiont (bacteria, fungi, or a combination of both) that modulates a mechanism to

15   maintain mosquito homeostasis. This mechanism might promote L-DOPA detoxification while

16   avoiding its conversion into dopamine, thereby regulating critical downstream processes in

17   insects, such as sclerotization, melanization, and the synthesis of neurotransmitters (e.g.,

18   tyramine and octopamine)[17,110]. Additionally, this scenario might align with the potential

19   modulation of gut microbiome composition, favoring the establishment of organisms that create a

20   cellular redox microenvironment, which enhances L-DOPA antioxidant properties. Further

21   research is needed to validate L-DOPA sequestration in *A. gambiae* and to assess its impact on

22   reproduction, exoskeleton stabilization, and protective role against environmental stressors such

23   as temperature, relative humidity, and UVA damage.

24   Our findings could be incorporated into mosquito control strategies. Despite strenuous measures

25   to mitigate vector-borne diseases, these still account for more than 700,000 deaths annually, of

26   which over 50% are caused by malaria - 96% of them in Africa [111]. As proposed by other groups,

27   the use of genetically modified mosquitoes to control malaria offers great hope but also comes

28   with concerns and controversy [112,113]. To effectively address these global risks and safeguard the

29   biosphere on which all species depend, it is imperative to develop novel, safe, and biodegradable

30   insecticides. Solutions derived from natural plant products hold promise in mitigating the impact

31   of chemical pesticides on the environment. L-DOPA, the plant phenolic precursor of dopamine, is

32   a neurotransmitter involved in several complex behaviors and processes in invertebrates,

33   including locomotion, learning, courtship, development, and melanin synthesis [51,114,115]. Native

34   plants from Africa such as banana [26] (*Musa balbisiana* Colla) and Fava beans (*Vicia faba)* [21,25],

1 contains up to 5% of L-DOPA in their leaves, flowers, and fruit parts. This metabolite is also a

2 non-protein amino acid usually shown to be toxic to many insects [66,116] that could drive trade-offs

3 between enhancing tolerance and life-history traits [18,19,114]. By fostering the development and

4 implementation of eco-friendly alternatives such as L-DOPA supplemented sugar baits designed

5 to specifically lure defined mosquito species and using natural body odor chemoattracts [117], it may

6 be possible to develop new tools for control of mosquito populations. Moreover, L-DOPA

7 supplementation of mosquito-infested waters could enhance their immunity to reduce parasite

8 burden and shorten lifespan, thus interfering with lifecycle and reducing the opportunity for

9 parasite transmission.

10 In summary, feeding of a sugar meal supplemented with L-DOPA to adult *A. gambiae* mosquitoes

11 augmented cuticular melanization and reduced parasite burden and lifespan. In addition to direct

12 L-DOPA effects, increased melanization has the potential to affect insect thermoregulation.

13 Consequently, L-DOPA supplementation has the potential for development as a novel, effective,

14 and environmentally safe strategy to eliminate and/or reduce malaria transmission, which merits

15 additional investigation including field studies of its usefulness and feasibility.

16 **Methods**

17

18 **Ethical statement**

19 The Johns Hopkins University Animal Care and Use Committee has approved this protocol, with

20 permit number MO18H82. Commercial anonymous human blood was used for parasite cultures

21 and mosquito feeding, and informed consent was therefore not applicable. The Johns Hopkins

22 School of Public Health Ethics Committee has approved this protocol. Mice for mosquito blood

23 feeding were housed in environmentally controlled rooms at 72°F and 42% humidity, with a 14.5-

24 h light/9.5-h dark cycle.

25

26 **Mosquito rearing**

27 Mosquitoes were obtained from colonies of *A. gambiae* (Keele strain) maintained in the insectary

28 of the Johns Hopkins Malaria Research Institute (JHMRI) on a 10% sucrose solution with 12-h

29 light/dark cycles at 27°C and 80% humidity under normal, non-sterile conditions. For most

30 experiments in this study, except for the oral toxicity analyses, newly emerged control and treated

31 mosquito groups were provided with 1.5% sucrose solutions in the absence or presence of the

32 melanin precursor supplement.

33

1 *Plasmodium falciparum* **culture**

2 *P. falciparum* NF54 asexual blood stage cultures were maintained *in vitro* according to the method

3 described earlier by Trager and Jenson (PMID 351412). Briefly, parasites were cultured in O+

4 erythrocytes at a 4% hematocrit in RPMI 1640 (Corning) supplemented with 2.1mM L-glutamine,

5 25mM HEPES, 0.72 mM hypoxanthine (Sigma), 0.21% w/v sodium bicarbonate (Sigma), and 10%

6 v/v heat-inactivated human serum (Interstate blood bank). Cultures were maintained at 37°C in a

7 glass candle jar. Gametocyte cultures were initiated at 0.5% asexual blood stage parasitemia and

8 at 4% hematocrit and maintained by changing the media daily for 17 d without the addition of fresh

9 blood to promote gametocytogenesis as described earlier [118]. Erythrocytes used for the study were

10 obtained from healthy donors under a Johns Hopkins Institutional Review Board-approved protocol

11 and were provided without identifiers to the laboratories.

12

13 **L-DOPA supplementation into sugar meal**

14 L-DOPA (3,4-Dihydroxy-L-phenylalanine) (Cat N° D9628) was obtained from Sigma-Aldrich.

15 Sterile sucrose solutions at 3% were diluted with an equal volume of sterile L-DOPA solutions and

16 prepared from a 5 mM stock in distilled water to obtain sugar solutions supplemented with L-DOPA

17 at concentrations ranging from 0.2 to 10 mM (0.4 to 20% w/w) L-DOPA. As control, 1.5% sucrose

18 solutions were prepared. This low sucrose concentration setup stemmed from an unintentionally

19 overdilution of sugar meals that revealed interesting and reproducible results, which we decided

20 to analyze.

21

22 **Survival assay**

23 Three- to four-day-old adult female *A. gambiae* were allowed to feed on sugar solutions prepared

24 as described above. Survival of mosquitoes was monitored for 14 d, and dead mosquitoes were

25 removed daily. Solutions containing 1.5% sucrose (end concentration) with an equal ratio of L-

26 DOPA were freshly prepared and provided every 2-3 d. To facilitate handling of paper cups with

27 mosquitoes (a group of 7, including sugar-only control), all cups were contained inside an airtight

28 plastic container and then incubated at 27°C inside a reach-in incubator.

29

30 **RNA extraction and transcriptional profiling**

31 Newly emerged adult female mosquitoes were allowed to feed with sugar solutions in the

32 presence and absence of 1 mM L-DOPA for 4 d. After this, mosquitoes were cold anesthetized to

33 remove their head using a tweezer over a glass plate on ice. Four groups of 10 headless

1 mosquitoes were transferred to a 1.5-ml tube. Midguts from four groups of 10 mosquitoes,

2 previously surface-sterilized, were dissected in a drop of sterile PBS and transferred to a 1.5-ml

3 tube containing 50 µl of sterile PBS. All samples were flash frozen in an ethanol/dry-ice bath and

4 stored at -80°C until RNA extraction.

5 Midguts and headless mosquitoes were homogenized in 1ml of Trizol with Lysing Matrix D Fast

6 Prep tubes in the FastPrep 24 (MP Bio), followed by RNA extraction using the PureLink RNA Mini

7 kit with on-column DNase treatment (ThermoFisher). RNA-Seq Libraries were prepared using the

8 Universal Plus mRNA-Seq Library prep kit (Tecan Genomics) incorporating unique dual indexes.

9 Libraries were assessed for quality by High Sensitivity D5000 ScreenTape on the 4200

10 TapeStation (Agilent Technologies). Quantification was performed with NuQuant reagent and by

11 Qubit High Sensitivity DNA assay, on Qubit 4 and Qubit Flex Fluorometers (Tecan

12 Genomics/ThermoFisher).

13 Libraries were diluted and an equimolar pool was prepared, according to the manufacturer's

14 protocol for appropriate sequencer. An Illumina iSeq Sequencer with iSeq100 i1 reagent V2 300

15 cycle kit was used for the final quality assessment of the library pool. For deep mRNA sequencing,

16 a 300 cycle (2 x 150 bp) Illumina NextSeq 500 (High) run was performed. Gene coverage was

17 about 40-50% with the average total reads at 24 million per sample. Three-to-four biological

18 replicates were analyzed for each condition for a total of 15 sequencing libraries. RNA-seq data

19 was analyzed with Partek Flow NGS Software as follows: pre-alignment QA/QC; alignment to *A.*

20 *gambiae* Reference Index using STAR 2.7.8a; post-alignment QA/QC; quantification of gene

21 counts to annotation model (Partek E/M); noise reduction filter by excluding features across

22 samples where maximum ≤10; normalization of gene counts using Median Rario (DESeq2 only,

23 Supplementary Data 2); and identification and comparison of differentially expressed genes with

24 DESeq2. Reference Genome: NCBI: GCA_000005575.1_AgamP3. From the resulting gene lists,

25 gene enrichment and pathway enrichment were performed within Partek Flow (Supplementary

26 Fig. 1b). Genes of interest were validated by q-RTPCR. All sequence files and sample information

27 have been deposited at NCBI Sequence Read Archive, NCBI BioProject: PRJNA1161683.

28

29 ***A. gambiae* infection with *P. falciparum*.**

30 Newly emerged adult female mosquitoes were allowed to feed on sugar solutions with up to 1

31 mM L-DOPA or dopamine for 4 d. On the fifth day, sugar meals were removed, and mosquitoes

32 were starved for 5-6 h prior to offering a *Plasmodium falciparum* NF54-laced blood meal with

33 gametocytemia 0.03%. Unfed mosquitoes were sorted, and blood-engorged mosquitoes were

34 further incubated for 8 d at 27 °C for oocyst counting. Midguts from *Pf*-infected mosquitoes were

1 dissected, stained with a 0.2% mercurochrome solution, and mounted on a slide with a coverslip

2 gently pressed on top to facilitate oocyst visualization. Enumeration of oocysts was performed

3 using a 20X objective under a Leica light microscope. For infections under aseptic conditions, the

4 artificial glass feeder membrane-feeding process was conducted under conditions as sterile as

5 possible to prevent antibiotic-treated mosquitoes from acquiring a bacterial infection [98].

6

7 ### *In vitro* susceptibility of *P. falciparum* NF54 to L-DOPA

8 To determine *P. falciparum* toxicity to L-DOPA, solutions at concentration up to 2 mM were freshly

9 prepared from a 5 mM L-DOPA stock. *P. falciparum* NF54 asexual and gametocyte stage cultures

10 were dispensed into 96 well plates and triplicate wells were treated with vehicle or L-DOPA at

11 concentrations of 0.25, 0.5, 1 and 2 mM for a total of 48 h. Blood smears were prepared after

12 drug treatment and asexual parasitemia or gametocytemia was calculated microscopically from

13 Giemsa-stained slides. The effect of L-DOPA exposure was determined by calculating %

14 decrease in number of parasites as compared to vehicle control.

15

16 ### Fungal challenge

17 *Cryptococcus neoformans* (strain H99-GFP) was cultured for 48 h in rich media at 30 °C with

18 moderate shaking. Yeast cells were collected, washed twice with PBS, and adjusted to a final

19 concentration of 1 x 10^8 cells/ ml. In parallel, newly emerged adult female mosquitoes were

20 allowed to feed with sugar solutions in the presence or absence of 1 mM L-DOPA for 4 d. Using

21 a nanoinjector, adult mosquitoes were injected intrathoracically with 69 µl of the fungal suspension

22 and then incubated at 19°C. Given that 1 mM L-DOPA triggers *C. neoformans* melanization

23 enhancing fungal fitness against biotic and abiotic stressors [119], to assess antifungal response in

24 *Anopheles* after infection, mosquitoes were surface sterilized 24 h post injection in 70% ethanol

25 for 3 min and rinsed twice in PBS for 2 min each time. Individual mosquitoes were transferred to

26 1.5-ml tubes containing 100 µl PBS and homogenized for 20 s using a sterile pestle. Two serial

27 dilutions of each sample were plated in Bird Seed agar (HiMedia Laboratories, PA), a selective

28 media for isolation and differentiation of *Cryptococcus* spp, and incubated at 30°C for 7 d, after

29 which the number of fungal colony-forming units (CFUs) were counted. Mosquito abdomens were

30 also dissected to visualize the presence of live (GPF-positive) or melanized and dead (GFP-

31 negative) *C. neoformans* yeasts, and images were captured using a Leica DM 2500 microscope.

32

33 ### Cuticle pigmentation

Newly emerged adult female mosquitoes were allowed to feed with L-DOPA solutions for up to 14 d as described above. For photography, mosquitoes were cold anesthetized, placed ventral side up on a slide under a dissection microscope, and imaged with an Iphone X under constant exposure and lighting conditions. Image analysis and pigment measurement were done as described previously [120]. Using the Fiji software [121], RGB color images were converted to 8-bit color, entire abdomens were selected using a freehand selection tool, and mean gray values were analyzed with the Measure tool. Pure black corresponds to 0 gray value whereas pure white equals 255.

Transmission Electron Microscopy

Newly emerged adult mosquitoes were allowed to feed with sucrose solutions, with and without supplementation of 1 mM L-DOPA for 7 d. Groups of 10 midlegs from each condition were dissected on a glass petri dish. To reduce hydrophobicity, legs were rinsed once in 70% ethanol, twice in PBS for 1 min each step, and then incubated overnight at 4°C in fixing solution containing 2% glutaraldehyde, 0.1 M sodium cacodylate (pH 7.4) and 2% paraformaldehyde in distilled water. After buffer rinse, samples were postfixed in 1% osmium tetroxide, 0.8% potassium ferrocyanide in 0.1 M sodium cacodylate for at least one hour (no more than two) on ice in the dark. After osmium, samples were rinsed in 100 mM maleate buffer, followed by uranyl acetate (2%) in 100 mM maleate (0.22 μm filtered, 1 h dark), dehydrated in a graded series of ethanol and embedded in a SPURR's/Eponate 12 (Ted Pella) resin. Samples were polymerized at 60C overnight. Thin sections, 60 to 90 nm, were cut with a diamond knife on the Reichert-Jung Ultracut E ultramicrotome and picked up with 2x1 mm formvar copper slot grids. To obtain consistent comparable segments across samples, femur cross-sections were obtained by conducting three sequential cuts at 200 nm depth into the femur from the direction of the tibia. Grids were stained with 2% uranyl acetate in 50% methanol followed by lead citrate and observed with a ThermoFisher Talos L120C at 120 kV. Images were captured with a ThermoFisher Ceta CCD (16 megapixel CMOS, 16-bit).

To account for differences in sequential cuts heterogeneity, at least three but no more than five representative images per cut were chosen per femur, each image captured ~18 μm of total cuticle length. A minimum of 3 measurements of total cuticle and endocuticle per image were taken at the same point and exocuticle was calculated by subtracting these values. Areas of the cuticle containing structural modifications were excluded from measurements.

1

Quantification of ^{13}C L-DOPA Melanin by Solid-State NMR

Newly emerged adult mosquitoes were allowed to feed with sucrose solutions, with and without supplementation with 1 mM of stable-isotope enriched ^{13}C L-DOPA (RING-^{13}C$_6$, 99%, CLM-1007-0, Cambridge Isotope Laboratories, MA, USA) for 7 d. Next, mosquitoes were sorted by sex, collected in 15-ml Falcon tubes, and lyophilized for 3 d. Solid-state NMR measurements were conducted on 8-10 mg samples using a Varian (Agilent) DirectDrive2 spectrometer operating at a ^{13}C frequency of 150 MHz and equipped with a 1.6-mm T3 HXY fast magic-angle spinning (fastMAS) probe spinning at 15.00 ± 0.02 kHz and a regulated temperature of 25 °C. ^{13}C NMR spectra of the lyophilized mosquito samples were obtained with 90° pulse lengths of 1.2 and 1.4 μs for ^{1}H and ^{13}C, respectively; 104-kHz heteronuclear decoupling using the small phase incremental alternation pulse sequence (SPINAL[122]) was applied during signal acquisition. Whereas a 10% linearly ramped ^{1}H amplitude, 1-ms time for ^{1}H-to-^{13}C polarization transfer, and 3-s delay between acquisitions were used to acquire CPMAS spectra that identified the carbon-containing functional groups, a longer 50-s delay was used for direct polarization (DPMAS) experiments that generated spectra with quantitatively reliable signal intensities. The CPMAS and DPMAS spectral runs required 4 and 56 hours, respectively.

Chitin measurements

The chitin content of adult mosquitoes post L-DOPA feeding for 7 d was determined based on the method of Lehmann and White (1975), [123] adapted as described previously used to quantify the chitin content of the cryptococcal cell wall material [124]. Using 15-ml tubes, 60 and 80 cold-anesthetized female and male mosquitoes, respectively, were freeze-dried, and lyophilized for 2-3 d. Mosquitoes were transferred to 1.5-ml microcentrifuge tubes, weighted (typically 14 and 11 mg, respectively), and homogenized in 200 μl of distilled water using a battery-operated homogenizer (3 20-sec cycles) and a horned sonicator at half amplitude (2 30-sec cycles). To solubilize and alkali-extract the samples, homogenates were centrifuged at 21,000 g for 5 min at room temperature and the pellet of each sample was resuspended in an equal volume (200 μl) of 3% (w/v) of sodium dodecyl sulfate (SDS). The samples were then incubated at 100 °C for 15 min and centrifuged again for 5 min after cooling. Next, after each pellet was washed twice with 200 μl distilled water, it was resuspended in 150 μl 2.1 M KOH. Samples were incubated at 80 °C for 90 min and cooled down to room temperature. After 400 μl 75% ethanol was added to each

1 sample, the sample was mixed and incubated on ice for 15 min. Sixty μl of a Celite 545 (Sigma-

2 Aldrich) suspension (1g of Celite 545 in 12.5 ml 75% ethanol, rested for 2 min) was then added

3 to each sample and centrifuged. The resultant cell matter was washed thoroughly once with 40%

4 ethanol, twice with PBS (pH 7), twice with distilled water, and resuspended in distilled water to a

5 final concentration of 10 mg ml $^{-1}$. To estimate the total amount of glucosamine stemming from

6 chitin plus chitosan, one 100 μl aliquot (equivalent to 1 mg dry weight) was transferred into a 2 ml

7 self-locking microcentrifuge tube and subjected to deacetylation with 100 μl 1 M HCl in a heating

8 block at 110 °C for 2 h. As a blank, one 100 μl of milliQ water was used instead of the mosquito

9 suspension. In a fume hood, sample deamination was achieved by adding 400 μl 2.5% $NaNO_2$,

10 then mixed and incubated for 15 min at room temperature to allow nitrogen oxides to dissipate.

11 After that, 200 μl of 12.5% ammonium sulfate was slowly added to each sample, vortexed, and

12 let stand at room temperature for 5 min. Measurement of hexosamines (amino sugars) from the

13 deacetylated samples was done by treatment with 3-methyl-2-benzothiazolone hydrazine

14 hydrochloride (MBTH, Sigma-Aldrich) under mildly acidic conditions. A 200 μl aliquot from each

15 sample was transferred to a 96-well plate and the absorbance at 650nm was recorded.

16 Concentrations were determined by comparison to a standard curve prepared from a 1mM

17 GlcNAc stock (Sigma-Aldrich) and ranging from 0 to 100 nM.

18 **Tarsal contact bioassay**

19 A susceptibility test against deltamethrin (0.05%) was done following the WHO protocol [125]. The

20 choice of deltamethrin, a pyrethroid insecticide, was justified by being one of the only two

21 insecticide classes approved for use on insecticide-treated bed nets (ITNs). Using an aspirator

22 22-25 *A. gambiae* female mosquitoes aged 2-5 d and previously allowed to feed on sucrose with

23 or without 1 mM L-DOPA supplementation for 4 d were introduced into two WHO holding tubes

24 (one test and one control) that contained untreated papers. Mosquitoes were allowed to settle

25 inside the tube for 15 min in an upright position, then with a quick and gentle tap mosquitoes were

26 transferred into the exposure tubes containing the insecticide-impregnated papers. Following

27 one-hour exposure at room temperature, mosquitoes were transferred back into holding tubes,

28 provided with a cotton pad moistened with 10 % sugar, and incubated at 27 °C. The number of

29 dead mosquitoes at 24 h was recorded. Control tubes contained oil-treated paper.

30

31 **Electron Paramagnetic Resonance (EPR) Spectroscopy**

1   Acid-resistant material attributable to melanin was isolated from *A. gambiae* mosquitoes fed with

2   and without 1 mM L-DOPA supplementation for 7 d following the protocol described previously

3   [126]. *Aedes aegypti* (mutant strain Yellow) and fungal eumelanin from *C. neoformans* were used

4   as negative and positive controls, respectively. EPR measurements were conducted at the

5   Caltech EPR Facility using a Bruker EMX X-band continuous-wave (CW) EPR spectrometer

6   equipped with a Bruker SHQE resonator. Samples were measured at room temperature under

7   non-saturating microwave power (4.4 µW) using a field modulation amplitude of 1 Gauss and

8   conversion time of 5 ms.

9

10   **Infrared thermography for mosquito bodies**

11   L-DOPA fed mosquitoes for 7 d were cold anesthetized, clustered into groups of ten on top of a

12   cooling block set at 0°C and arranged from left to right for increasing L-DOPA concentrations for

13   up to 1 mM. Basal mosquito temperatures were recorded in dark conditions using an infrared (IR)

14   camera (FLIR Systems, Wilsonville, OR) mounted 40 cm above the cooling block setup on a

15   benchtop in a temperature-controlled room (22 ± 5°C, 50% relative humidity). Irradiations were

16   conducted for 4 min using a white LED lamp (250 W, 1850 Lumens, PAR38HO-E26-19W-4000K-

17   25°, Green Creative) mounted 40 cm above the cooling block and resulting in an average

18   luminance of ~415 LUX. The optimal LED bulb positioning for homogeneous light exposure was

19   calculated based on the light intensity distribution using graph paper and a light meter

20   (**Supplementary Fig. 5**).

21

22   **Fecundity, egg hatching rate and life span.**

23   For the fecundity assay, newly emerged adult female *A. gambiae* were allowed to feed on a sugar

24   solution supplemented with 1mM L-DOPA for 7 d, whereas the controls were fed 1.5% sucrose

25   without L-DOPA. Mosquitoes were allowed to blood-feed on mice for 20 min and then

26   anesthetized on ice; all non-engorged mosquitoes were discarded. At 3 d post blood meal,

27   individual mosquitoes were transferred to a 50-ml Falcon tube containing a paper cup in the

28   bottom halfway submerged into clean distilled water for oviposition. The number of eggs laid by

29   each mosquito was recorded for up to 4 d under a light microscope. Female mosquitoes that died

30   before oviposition were not included in the study. After each count, adult mosquitoes were

31   removed from the vials, eggs were completely submerged into larval rearing water, and vials were

32   incubated for 3-4 d at 27°C and 30°C, making sure that the paper cups remained moistened. The

33   first and second instar larvae were counted under a light microscope.

The life span of *A. gambiae* females during continued exposure to a sugar meal supplemented with 1 mM L-DOPA was measured by placing newly emerged mosquitoes into paper cups with a sugar solution that was freshly prepared every 2-3 d. Dead mosquitoes were recorded and removed daily until no live mosquitoes remained. For this experimental setting, control and 1mM L-DOPA cups were directly incubated inside the reach-in incubator. Survival analysis represents pooled data from three biological replicates of 35 mosquitoes each.

Dopamine measurements

Dopamine quantification was conducted from whole female mosquitoes post L-DOPA feeding and from bacterial supernatants.

Sample collection: For mosquito samples, newly emerged adult mosquitoes were allowed to feed with sugar solutions supplemented with L-DOPA at three different concentrations (0.2 mM, 0.6 mM, and 1 mM) for 4 d. At the assayed time, five whole female mosquitoes were collected in 1.5-ml brown tubes and flash-frozen in an ethanol-dry ice bath. Mosquito supernatants containing both hemolymph and cuticle dopamine were obtained by adding 200 µl ice-cold 0.2 M perchloric acid to each tube, homogenizing for 20 s on ice, and centrifuging at 20,000 g for 10 min at 4 °C [127]. Supernatants (~100 µl) were transferred to a new brown 1.5-ml tube and kept at -80 °C until further processing was conducted. For bacterial samples, a single colony of each bacterial strain, previously shown to induce fungal melanization, was grown in LB broth at 30 °C for 96 h. Filter sterilized, cell-free culture supernatants were acidified to pH 4 with 1 M HCl, fractionated by FPLC using an AKTA Pure liquid chromatograph with a UV-900 monitor to measure absorbance at 214 nm (Amersham Biosciences) and a C18 reverse-phase column (Phenomenex Luna 5 µm, 100 Å, LC Column 150 x 4.6 mm) using an isocratic mobile phase of 25 mM potassium phosphate buffer (pH 3.1) at a flow rate of 1.0 ml/min [53]. Fractions of 200 µl were collected into a new brown 1.5-ml tube and kept at -80 °C until further processing was conducted; a 50 mM dopamine (Sigma-Aldrich) solution was used as standard.

Sample preparation and derivatization: Dopamine standards were prepared in 10 µg/mL sodium metabisulfite in water. Samples were derivatized as described previously, with the following adjustments: 20 µL of standards and samples were transferred to an extraction plate; 10 µL of 100 mM sodium tetraborate in water and 5 µL of a cold internal standard solution consisting of 500 ng/mL dopamine-d3 in acetonitrile (v/v) were added to each sample and mixed for 1 min on plate shaker at 1,600 rpm; 10 µL of 2% benzoyl chloride in acetonitrile (v/v) was then

24

1 added to each sample and the plate was mixed for 2 min at 1,600 rpm. 10µL of 1% formic acid in

2 water (v/v) was added to quench the reaction. 1µL of each sample was injected for analysis.

3 **Sample analysis:** Samples were analyzed using an Agilent 6540 QTOF with a Jet Stream

4 Electrospray Ionization Source (ESI) and an Agilent 1290 UHPLC (Agilent Technologies, Santa

5 Clara, CA). Solvents were 10 mM ammonium formate in water (A) and acetonitrile (B). The

6 samples were kept at 10°C during analysis. Chromatographic separation was achieved over 3.0

7 minutes using a Phenomenex Luna Omega 2.1 x 100mm, 1.6µm, C18 column at 40°C with a

8 binary gradient starting with 10% B. The LC gradient was as follows: 0–1.2 min, 10% - 95% B; 1.2

9 - 2.0 min, 95% B; 2.01, 10% B. The flow rate was 400 µl min^{-1}. Mass spectral acquisition was

10 performed using full scan MS from *m/z* 100 to 1000 with the following source conditions: Drying

11 and Sheath Gas temperatures of 350°C and 400°C, respectively; both gas flows at 12L/min;

12 Nebulizer- 45psig, VCap, Nozzle and Fragmenter voltages at 3000 V, 600 V and 100 V,

13 respectively. Proton adducts of the triple benzoylated dopamine and dopamine-d$_3$ (*m/z* 466.1649

14 and 469.1837, respectively) were extracted within a +/- 20 ppm window. Analyte peak areas were

15 determined from the extracted ion chromatograms and concentrations were calculated by linear

16 regression analysis using Agilent Masshunter Quantitative Analysis Software (B.08.00). Limit of

17 quantification was 1.0 ng/ml.

18

19 **Plate confrontation assays**

20 As a proxy for the ability to synthesize catecholamines from bacteria isolated from the midgut of

21 wild-caught *An. aranbiensis* and *Ae. aegypti* adult mosquitoes as well as an environmental source

22 relevant to mosquito aquatic stages, we monitored Cryptococcal melanization as previously

23 reported [53].

24

25 **Statistical Analysis**

26 Data were graphed and analyzed for statistical significance using GraphPad Prism 10 (version

27 10.0.1) software (GraphPad Software, LLC). Particular tests used for experiments are indicated

28 in the legend of each respective figure.

29

30 **Data availability**

All data generated or analyzed during this study are included in this published article (and its Supplementary files). The datasets presented in this manuscript are publicly available Figshare data repository at 10.6084/m9.figshare.27122907 and 10.6084/m9.figshare.28063112**.** The RNAseq data was submitted to the Sequence Read Archive (SRA) database (PRJNA1161683).

References

1   Klepac, P. *et al.* Climate change, malaria and neglected tropical diseases: a scoping review. *Trans R Soc Trop Med Hyg*, doi:10.1093/trstmh/trae026 (2024).

2   Caminade, C. *et al.* Impact of climate change on global malaria distribution. *Proc Natl Acad Sci U S A* **111**, 3286-3291, doi:10.1073/pnas.1302089111 (2014).

3   Kulkarni, M. A. *et al.* 10 Years of Environmental Change on the Slopes of Mount Kilimanjaro and Its Associated Shift in Malaria Vector Distributions. *Front Public Health* **4**, 281, doi:10.3389/fpubh.2016.00281 (2016).

4   Bagcchi, S. Locally acquired malaria cases in the USA. *Lancet Infect Dis* **23**, e401, doi:10.1016/S1473-3099(23)00581-9 (2023).

5   Carlson, C. J., Bannon, E., Mendenhall, E., Newfield, T. & Bansal, S. Rapid range shifts in African Anopheles mosquitoes over the last century. *Biol Lett* **19**, 20220365, doi:10.1098/rsbl.2022.0365 (2023).

6   Suh, P. F. *et al.* Impact of insecticide resistance on malaria vector competence: a literature review. *Malar J* **22**, 19, doi:10.1186/s12936-023-04444-2 (2023).

7   Takken, W. & Lindsay, S. Increased Threat of Urban Malaria from Anopheles stephensi Mosquitoes, Africa. *Emerg Infect Dis* **25**, 1431-1433, doi:10.3201/eid2507.190301 (2019).

8   Organization, W. H. Global Vector Control Response 2017–2030. . (Geneva, Switzerland: World Health Organization. , 2017).

9   Wilson, A. L. *et al.* The importance of vector control for the control and elimination of vector-borne diseases. *PLoS Negl Trop Dis* **14**, e0007831, doi:10.1371/journal.pntd.0007831 (2020).

10   Bhatt, S. *et al.* The effect of malaria control on Plasmodium falciparum in Africa between 2000 and 2015. *Nature* **526**, 207-211, doi:10.1038/nature15535 (2015).

11   Protopopoff, N. *et al.* Effectiveness of a long-lasting piperonyl butoxide-treated insecticidal net and indoor residual spray interventions, separately and together, against malaria transmitted by pyrethroid-resistant mosquitoes: a cluster, randomised controlled, two-by-two factorial design trial. *Lancet* **391**, 1577-1588, doi:10.1016/S0140-6736(18)30427-6 (2018).

12   Barredo, E. & DeGennaro, M. Not Just from Blood: Mosquito Nutrient Acquisition from Nectar Sources. *Trends Parasitol* **36**, 473-484, doi:10.1016/j.pt.2020.02.003 (2020).

13   Fiorenzano, J. M., Koehler, P. G. & Xue, R. D. Attractive Toxic Sugar Bait (ATSB) For Control of Mosquitoes and Its Impact on Non-Target Organisms: A Review. *Int J Environ Res Public Health* **14**, doi:10.3390/ijerph14040398 (2017).

14   Lovett, B. *et al.* Transgenic Metarhizium rapidly kills mosquitoes in a malaria-endemic region of Burkina Faso. *Science* **364**, 894-897, doi:10.1126/science.aaw8737 (2019).

15   Bilgo, E. *et al.* Field assessment of potential sugar feeding stations for disseminating bacteria in a paratransgenic approach to control malaria. *Malar J* **17**, 367, doi:10.1186/s12936-018-2516-x (2018).

16   Cirimotich, C. M. *et al.* Natural microbe-mediated refractoriness to Plasmodium infection in Anopheles gambiae. *Science* **332**, 855-858, doi:10.1126/science.1201618 (2011).

17   Sugumaran, M. & Barek, H. Critical Analysis of the Melanogenic Pathway in Insects and Higher Animals. *Int J Mol Sci* **17**, doi:10.3390/ijms17101753 (2016).

18   Zhang, Y. *et al.* Pea aphid Acyrthosiphon pisum sequesters plant-derived secondary metabolite L-DOPA for wound healing and UVA resistance. *Sci Rep* **6**, 23618, doi:10.1038/srep23618 (2016).

19   Lanno, S. M. *et al.* Genomics Analysis of L-DOPA Exposure in Drosophila sechellia. *G3 (Bethesda)* **9**, 3973-3980, doi:10.1534/g3.119.400552 (2019).

20   Wu, K. *et al.* Plant phenolics are detoxified by prophenoloxidase in the insect gut. *Sci Rep* **5**, 16823, doi:10.1038/srep16823 (2015).

21   Topal, N., Bulduk, I., Mut, Z., Bozoglu, H. & Tosun, Y. K. Flowers, Pollen and Honey for Use in the Treatment of Parkinson's Disease. *Rev Chim* **71**, 308-319, doi:https://doi.org/10.37358/RC.20.9.8341 (2020).

22   Barda, M. *et al.* Flower morphology and nectar quality traits in faba bean affect attraction to bees. *Journal of Applied Entomology* **148**, 57-73, doi:https://doi.org/10.1111/jen.13208 (2023).

23   Jhumur, U. S., Dötterl, S. & Jürgens, A. Electrophysiological and behavioural responses of mosquitoes to volatiles of Silene otites (Caryophyllaceae). *Arthropod-Plant Interactions* **1**, 245-254, doi:10.1007/s11829-007-9022-3 (2007).

24   Huff, R. M. & Pitts, R. J. An odorant receptor from Anopheles gambiae that demonstrates enantioselectivity to the plant volatile, linalool. *PLoS One* **14**, e0225637, doi:10.1371/journal.pone.0225637 (2019).

25   Gish, M., Mescher, M. C. & De Moraes, C. M. Targeted predation of extrafloral nectaries by insects despite localized chemical defences. *Proc Biol Sci* **282**, 20151835, doi:10.1098/rspb.2015.1835 (2015).

26   Khayhan, K. *et al.* Banana blossom agar (BABA), a new medium to isolate members of the Cryptococcus neoformans/Cryptococcus gattii species complex useful for resource limited countries. *Mycoses* **61**, 959-962, doi:10.1111/myc.12833 (2018).

27   Soares, A. R. *et al.* The role of L-DOPA in plants. *Plant Signal Behav* **9**, e28275 (2014).

28   Yang, X., Zhang, X. & Zhou, R. Determination of l-Dopa Content and Other Significant Nitrogenous Compounds in the Seeds of Seven Mucuna and Stizolobium Species in China. *Pharmaceutical Biology* **39**, 312-316, doi:10.1076/phbi.39.4.312.5905 (2001).

29   Goyoaga, C. *et al.* Content and distribution of vicine, convicine and L-DOPA during germination and seedling growth of two Vicia faba L. varieties. *Eur Food Res Technol* **227**, 1537-1542, doi:10.1007/s00217-008-0876-0 (2008).

30   Etemadi, F., Hashemi, M., Randhir, R., ZandVakili, O. & Ebadi, A. Accumulation of l-DOPA in various organs of faba bean and influence of drought, nitrogen stress, and processing methods on l-DOPA yield. `The Crop Journal* **6**, 426-434, doi:https://doi.org/10.1016/j.cj.2017.12.001 (2018).

31   Zhang, W. *et al.* Regulators and signalling in insect antimicrobial innate immunity: Functional molecules and cellular pathways. *Cell Signal* **83**, 110003, doi:10.1016/j.cellsig.2021.110003 (2021).

32   Kouamo, M. F. M. *et al.* Genome-Wide Transcriptional Analysis and Functional Validation Linked a Cluster of Epsilon Glutathione S-Transferases with Insecticide Resistance in the Major Malaria Vector Anopheles funestus across Africa. *Genes (Basel)* **12**, doi:10.3390/genes12040561 (2021).

33   Kwon, H., Mohammed, M., Franzen, O., Ankarklev, J. & Smith, R. C. Single-cell analysis of mosquito hemocytes identifies signatures of immune cell subtypes and cell differentiation. *Elife* **10**, doi:10.7554/eLife.66192 (2021).

27

34   Yassine, H., Kamareddine, L. & Osta, M. A. The mosquito melanization response is implicated in defense against the entomopathogenic fungus Beauveria bassiana. *PLoS Pathog* **8**, e1003029, doi:10.1371/journal.ppat.1003029 (2012).

35   El Moussawi, L., Nakhleh, J., Kamareddine, L. & Osta, M. A. The mosquito melanization response requires hierarchical activation of non-catalytic clip domain serine protease homologs. *PLoS Pathog* **15**, e1008194, doi:10.1371/journal.ppat.1008194 (2019).

36   Smith, D. F. Q., Dragotakes, Q., Kulkarni, M., Hardwick, J. M. & Casadevall, A. Galleria mellonella immune melanization is fungicidal during infection. *Commun Biol* **5**, 1364, doi:10.1038/s42003-022-04340-6 (2022).

37   Vizioli, J. *et al.* Gambicin: a novel immune responsive antimicrobial peptide from the malaria vector Anopheles gambiae. *Proc Natl Acad Sci U S A* **98**, 12630-12635, doi:10.1073/pnas.221466798 (2001).

38   Smith, R. C. *et al.* Molecular Profiling of Phagocytic Immune Cells in Anopheles gambiae Reveals Integral Roles for Hemocytes in Mosquito Innate Immunity. *Mol Cell Proteomics* **15**, 3373-3387, doi:10.1074/mcp.M116.060723 (2016).

39   Wigglesworth, V. B. The insect cuticle. *Biol Rev Camb Philos Soc* **23**, 408-451, doi:10.1111/j.1469-185x.1948.tb00566.x (1948).

40   Sealy, R. C., Hyde, J. S., Felix, C. C., Menon, I. A. & Prota, G. Eumelanins and pheomelanins: characterization by electron spin resonance spectroscopy. *Science* **217**, 545-547, doi:10.1126/science.6283638 (1982).

41   Li, M. *et al.* Germline Cas9 expression yields highly efficient genome engineering in a major worldwide disease vector, Aedes aegypti. *Proc Natl Acad Sci U S A* **114**, E10540-E10549, doi:10.1073/pnas.1711538114 (2017).

42   Camacho, E. *et al.* N-acetylglucosamine affects Cryptococcus neoformans cell-wall composition and melanin architecture. *Microbiology* **163**, 1540-1556, doi:10.1099/mic.0.000552 (2017).

43   Wood, O., Hanrahan, S., Coetzee, M., Koekemoer, L. & Brooke, B. Cuticle thickening associated with pyrethroid resistance in the major malaria vector Anopheles funestus. *Parasit Vectors* **3**, 67, doi:10.1186/1756-3305-3-67 (2010).

44   Yahouedo, G. A. *et al.* Contributions of cuticle permeability and enzyme detoxification to pyrethroid resistance in the major malaria vector Anopheles gambiae. *Sci Rep* **7**, 11091, doi:10.1038/s41598-017-11357-z (2017).

45   Cordero, R. J. B. *et al.* Impact of Yeast Pigmentation on Heat Capture and Latitudinal Distribution. *Curr Biol* **28**, 2657-2664 e2653, doi:10.1016/j.cub.2018.06.034 (2018).

46   True, J. R. Insect melanism: the molecules matter. *Trends in Ecology and Evolution* **18**, 640-647 (2003).

47   Zeuss, D., Brandl, R., Brandle, M., Rahbek, C. & Brunzel, S. Global warming favours light-coloured insects in Europe. *Nat Commun* **5**, 3874, doi:10.1038/ncomms4874 (2014).

48   Haque, M. T., Khan, M. K. & Herberstein, M. E. Current evidence of climate-driven colour change in insects and its impact on sexual signals. *Ecol Evol* **14**, e11623, doi:10.1002/ece3.11623 (2024).

49   Gonzalez-Tokman, D. *et al.* Insect responses to heat: physiological mechanisms, evolution and ecological implications in a warming world. *Biol Rev Camb Philos Soc* **95**, 802-821, doi:10.1111/brv.12588 (2020).

50   d'Ischia, M. *et al.* Melanins and melanogenesis: from pigment cells to human health and technological applications. *Pigment Cell Melanoma Res* **28**, 520-544, doi:10.1111/pcmr.12393 (2015).

51   Barek, H., Sugumaran, M., Ito, S. & Wakamatsu, K. Insect cuticular melanins are distinctly different from those of mammalian epidermal melanins. *Pigment Cell Melanoma Res* **31**, 384-392, doi:10.1111/pcmr.12672 (2018).

52 Fukumitsu, Y. *et al.* Elevation of dopamine level reduces host-seeking activity in the adult female mosquito Aedes albopictus. *Parasit Vectors* **5**, 92, doi:10.1186/1756-3305-5-92 (2012).

53 Frases, S., Chaskes, S., Dadachova, E. & Casadevall, A. Induction by Klebsiella aerogenes of a melanin-like pigment in Cryptococcus neoformans. *Appl Environ Microbiol* **72**, 1542-1550, doi:10.1128/AEM.72.2.1542-1550.2006 (2006).

54 Hegde, S. *et al.* Interkingdom interactions shape the fungal microbiome of mosquitoes. *Anim Microbiome* **6**, 11, doi:10.1186/s42523-024-00298-4 (2024).

55 Tawidian, P., Coon, K. L., Jumpponen, A., Cohnstaedt, L. W. & Michel, K. Host-Environment Interplay Shapes Fungal Diversity in Mosquitoes. *mSphere* **6**, e0064621, doi:10.1128/mSphere.00646-21 (2021).

56 Chatterjee, S., Prados-Rosales, R., Itin, B., Casadevall, A. & Stark, R. E. Solid-state NMR Reveals the Carbon-based Molecular Architecture of Cryptococcus neoformans Fungal Eumelanins in the Cell Wall. *J Biol Chem* **290**, 13779-13790, doi:10.1074/jbc.M114.618389 (2015).

57 Ramirez, J. L. *et al.* Reciprocal tripartite interactions between the Aedes aegypti midgut microbiota, innate immune system and dengue virus influences vector competence. *PLoS Negl Trop Dis* **6**, e1561, doi:10.1371/journal.pntd.0001561 (2012).

58 Wells, J. S. *et al.* SQ 26,180, a novel monobactam. I Taxonomy, fermentation and biological properties. *J Antibiot (Tokyo)* **35**, 184-188, doi:10.7164/antibiotics.35.184 (1982).

59 Chernin, L. S. *et al.* Chitinolytic activity in Chromobacterium violaceum: substrate analysis and regulation by quorum sensing. *J Bacteriol* **180**, 4435-4441, doi:10.1128/JB.180.17.4435-4441.1998 (1998).

60 Hillyer, J. F. Insect immunology and hematopoiesis. *Dev Comp Immunol* **58**, 102-118, doi:10.1016/j.dci.2015.12.006 (2016).

61 Clayton, A. M., Dong, Y. & Dimopoulos, G. The Anopheles innate immune system in the defense against malaria infection. *J Innate Immun* **6**, 169-181, doi:10.1159/000353602 (2014).

62 Saraiva, R. G., Kang, S., Simoes, M. L., Anglero-Rodriguez, Y. I. & Dimopoulos, G. Mosquito gut antiparasitic and antiviral immunity. *Dev Comp Immunol* **64**, 53-64, doi:10.1016/j.dci.2016.01.015 (2016).

63 Liao, C., Upadhyay, A., Liang, J., Han, Q. & Li, J. 3,4-Dihydroxyphenylacetaldehyde synthase and cuticle formation in insects. *Dev Comp Immunol* **83**, 44-50, doi:10.1016/j.dci.2017.11.007 (2018).

64 Vavricka, C. *et al.* From L-dopa to dihydroxyphenylacetaldehyde: a toxic biochemical pathway plays a vital physiological function in insects. *PLoS One* **6**, e16124, doi:10.1371/journal.pone.0016124 (2011).

65 Goldstein, D. S. The Catecholaldehyde Hypothesis for the Pathogenesis of Catecholaminergic Neurodegeneration: What We Know and What We Do Not Know. *Int J Mol Sci* **22**, doi:10.3390/ijms22115999 (2021).

66 Renault, D., Dorrah, M. A., Mohamed, A. A., Abdelfattah, E. A. & Bassal, T. T. Assessment of oxidative stress and activities of antioxidant enzymes depicts the negative systemic effect of iron-containing fertilizers and plant phenolic compounds in the desert locust. *Environ Sci Pollut Res Int* **23**, 21989-22000, doi:10.1007/s11356-016-7391-9 (2016).

67 Calabrese, E. J. & Baldwin, L. A. Agonist consentration gradients as a generalizable regulatory implementation Strategy. *Crit Rev Toxicol* **31**, 471-473, doi:10.1080/20014091111758 (2001).

68 Calabrese, E. J. & Mattson, M. P. How does hormesis impact biology, toxicology, and medicine? *NPJ Aging Mech Dis* **3**, 13, doi:10.1038/s41514-017-0013-z (2017).

69 Schirrmacher, V. Less Can Be More: The Hormesis Theory of Stress Adaptation in the Global Biosphere and Its Implications. *Biomedicines* **9**, doi:10.3390/biomedicines9030293 (2021).

70   Ali, M., Al-Olayan, E. M., Lewis, S., Matthews, H. & Hurd, H. Naturally occurring triggers that induce apoptosis-like programmed cell death in Plasmodium berghei ookinetes. *PLoS One* **5**, doi:10.1371/journal.pone.0012634 (2010).

71   Foster, W. A. Mosquito sugar feeding and reproductive energetics. *Annu Rev Entomol* **40**, 443-474, doi:10.1146/annurev.en.40.010195.002303 (1995).

72   Wang, M. *et al.* Glucose-mediated proliferation of a gut commensal bacterium promotes Plasmodium infection by increasing mosquito midgut pH. *Cell Rep* **35**, 108992, doi:10.1016/j.celrep.2021.108992 (2021).

73   Magistrado, D., El-Dougdoug, N. K. & Short, S. M. Sugar restriction and blood ingestion shape divergent immune defense trajectories in the mosquito Aedes aegypti. *Sci Rep* **13**, 12368, doi:10.1038/s41598-023-39067-9 (2023).

74   Weger, A. A. & Rittschof, C. C. The diverse roles of insulin signaling in insect behavior. *Front Insect Sci* **4**, 1360320, doi:10.3389/finsc.2024.1360320 (2024).

75   Ferreira, A. & Milan, M. Dally Proteoglycan Mediates the Autonomous and Nonautonomous Effects on Tissue Growth Caused by Activation of the PI3K and TOR Pathways. *PLoS Biol* **13**, e1002239, doi:10.1371/journal.pbio.1002239 (2015).

76   Perez-Hedo, M., Rivera-Perez, C. & Noriega, F. G. The insulin/TOR signal transduction pathway is involved in the nutritional regulation of juvenile hormone synthesis in Aedes aegypti. *Insect Biochem Mol Biol* **43**, 495-500, doi:10.1016/j.ibmb.2013.03.008 (2013).

77   Regan, J. C., Froy, H., Walling, C. A., Moatt, J. P. & Nussey, D. H. Dietary restriction and insulin-like signalling pathways as adaptive plasticity: A synthesis and re-evaluation. *Functional Ecology* **34**, 107-128, doi:https://doi.org/10.1111/1365-2435.13418 (2019).

78   Huang, C. Y., Chou, S. Y., Bartholomay, L. C., Christensen, B. M. & Chen, C. C. The use of gene silencing to study the role of dopa decarboxylase in mosquito melanization reactions. *Insect Mol Biol* **14**, 237-244, doi:10.1111/j.1365-2583.2004.00552.x (2005).

79   Takahashi, A. Pigmentation and behavior: potential association through pleiotropic genes in Drosophila. *Genes Genet Syst* **88**, 165-174, doi:10.1266/ggs.88.165 (2013).

80   Li, J., Zhao, X. & Christensen, B. M. Dopachrome conversion activity in Aedes aegypti: significance during melanotic encapsulation of parasites and cuticular tanning. *Insect Biochem Mol Biol* **24**, 1043-1049, doi:10.1016/0965-1748(94)90142-2 (1994).

81   McKay, J. K., Richards, J. H. & Mitchell-Olds, T. Genetics of drought adaptation in Arabidopsis thaliana: I. Pleiotropy contributes to genetic correlations among ecological traits. *Mol Ecol* **12**, 1137-1151, doi:10.1046/j.1365-294x.2003.01833.x (2003).

82   Balabanidou, V. *et al.* Cytochrome P450 associated with insecticide resistance catalyzes cuticular hydrocarbon production in Anopheles gambiae. *Proc Natl Acad Sci U S A* **113**, 9268-9273, doi:10.1073/pnas.1608295113 (2016).

83   Balabanidou, V. *et al.* Mosquitoes cloak their legs to resist insecticides. *Proc Biol Sci* **286**, 20191091, doi:10.1098/rspb.2019.1091 (2019).

84   Pedrini, N. *et al.* Control of pyrethroid-resistant Chagas disease vectors with entomopathogenic fungi. *PLoS Negl Trop Dis* **3**, e434, doi:10.1371/journal.pntd.0000434 (2009).

85   Liu, N. Insecticide resistance in mosquitoes: impact, mechanisms, and research directions. *Annu Rev Entomol* **60**, 537-559, doi:10.1146/annurev-ento-010814-020828 (2015).

86   Bonizzoni, M. *et al.* RNA-seq analyses of changes in the Anopheles gambiae transcriptome associated with resistance to pyrethroids in Kenya: identification of candidate-resistance genes and candidate-resistance SNPs. *Parasit Vectors* **8**, 474, doi:10.1186/s13071-015-1083-z (2015).

87   Chrissian, C. *et al.* Melanin deposition in two Cryptococcus species depends on cell-wall composition and flexibility. *J Biol Chem* **295**, 1815-1828, doi:10.1074/jbc.RA119.011949 (2020).

88   Stuart-Fox, D., Newton, E. & Clusella-Trullas, S. Thermal consequences of colour and near-infrared reflectance. *Philos Trans R Soc Lond B Biol Sci* **372**, doi:10.1098/rstb.2016.0345 (2017).

89   Freoa, L. *et al.* Drosophilids with darker cuticle have higher body temperature under light. *Sci Rep* **13**, 3513, doi:10.1038/s41598-023-30652-6 (2023).

90   Sibilia, C. D. *et al.* Thermal Physiology and Developmental Plasticity of Pigmentation in the Harlequin Bug (Hemiptera: Pentatomidae). *J Insect Sci* **18**, doi:10.1093/jisesa/iey066 (2018).

91   Lopez, V. M. *et al.* Color lightness of velvet ants (Hymenoptera: Mutillidae) follows an environmental gradient. *J Therm Biol* **100**, 103030, doi:10.1016/j.jtherbio.2021.103030 (2021).

92   Agyekum, T. P. *et al.* A Systematic Review of the Effects of Temperature on Anopheles Mosquito Development and Survival: Implications for Malaria Control in a Future Warmer Climate. *Int J Environ Res Public Health* **18**, doi:10.3390/ijerph18147255 (2021).

93   Nunes, R. D. *et al.* Polyphenol-Rich Diets Exacerbate AMPK-Mediated Autophagy, Decreasing Proliferation of Mosquito Midgut Microbiota, and Extending Vector Lifespan. *PLoS Negl Trop Dis* **10**, e0005034, doi:10.1371/journal.pntd.0005034 (2016).

94   Blomquist, G. J. & Ginzel, M. D. Chemical Ecology, Biochemistry, and Molecular Biology of Insect Hydrocarbons. *Annu Rev Entomol* **66**, 45-60, doi:10.1146/annurev-ento-031620-071754 (2021).

95   Gibbs, A. & Pomonis, J. G. Physical properties of insect cuticular hydrocarbons: The effects of chain length, methyl-branching and unsaturation. *Comparative Biochemistry and Physiology Part B: Biochemistry and Molecular Biology* **112**, 243-249, doi:https://doi.org/10.1016/0305-0491(95)00081-X (1995).

96   Cirstea, M. S. *et al.* A novel pathway of levodopa metabolism by commensal Bifidobacteria. *Sci Rep* **13**, 19155, doi:10.1038/s41598-023-45953-z (2023).

97   van Kessel, S. P. *et al.* Gut bacterial tyrosine decarboxylases restrict levels of levodopa in the treatment of Parkinson's disease. *Nat Commun* **10**, 310, doi:10.1038/s41467-019-08294-y (2019).

98   Dong, Y., Manfredini, F. & Dimopoulos, G. Implication of the mosquito midgut microbiota in the defense against malaria parasites. *PLoS Pathog* **5**, e1000423, doi:10.1371/journal.ppat.1000423 (2009).

99   Saraiva, R. G. & Dimopoulos, G. Bacterial natural products in the fight against mosquito-transmitted tropical diseases. *Nat Prod Rep* **37**, 338-354, doi:10.1039/c9np00042a (2020).

100   Roshchina, V. V. New Trends and Perspectives in the Evolution of Neurotransmitters in Microbial, Plant, and Animal Cells. *Adv Exp Med Biol* **874**, 25-77, doi:10.1007/978-3-319-20215-0_2 (2016).

101   Zhao, M., Lin, X. & Guo, X. The Role of Insect Symbiotic Bacteria in Metabolizing Phytochemicals and Agrochemicals. *Insects* **13**, doi:10.3390/insects13070583 (2022).

102   Shamjana, U., Vasu, D. A., Hembrom, P. S., Nayak, K. & Grace, T. The role of insect gut microbiota in host fitness, detoxification and nutrient supplementation. *Antonie Van Leeuwenhoek* **117**, 71, doi:10.1007/s10482-024-01970-0 (2024).

103   El-Shehawy, R., Luecke-Johansson, S., Ribbenstedt, A. & Gorokhova, E. Microbiota-Dependent and -Independent Production of l-Dopa in the Gut of Daphnia magna. *mSystems* **6**, e0089221, doi:10.1128/mSystems.00892-21 (2021).

104   Briggs, A. M. *et al.* Anopheles stephensi Feeding, Flight Behavior, and Infection With Malaria Parasites are Altered by Ingestion of Serotonin. *Front Physiol* **13**, 911097, doi:10.3389/fphys.2022.911097 (2022).

105   Shim, J., Mukherjee, T. & Banerjee, U. Direct sensing of systemic and nutritional signals by haematopoietic progenitors in Drosophila. *Nat Cell Biol* **14**, 394-400, doi:10.1038/ncb2453 (2012).

106   Beran, F. & Petschenka, G. Sequestration of Plant Defense Compounds by Insects: From Mechanisms to Insect-Plant Coevolution. *Annu Rev Entomol* **67**, 163-180, doi:10.1146/annurev-ento-062821-062319 (2022).

107   Jeckel, A. M. *et al.* Metabolization and sequestration of plant specialized metabolites in insect herbivores: Current and emerging approaches. *Front Physiol* **13**, 1001032, doi:10.3389/fphys.2022.1001032 (2022).

108   Opitz, S. E. W. & Müller, C. Plant chemistry and insect sequestration. *Chemoecology* **19**, 117-154, doi:10.1007/s00049-009-0018-6 (2009).

109   De Marco, L. *et al.* The choreography of the chemical defensome response to insecticide stress: insights into the Anopheles stephensi transcriptome using RNA-Seq. *Sci Rep* **7**, 41312, doi:10.1038/srep41312 (2017).

110   Roeder, T. Tyramine and octopamine: ruling behavior and metabolism. *Annu Rev Entomol* **50**, 447-477, doi:10.1146/annurev.ento.50.071803.130404 (2005).

111   Organization, W. H. World Malaria Report 2021. 322 (World Health Organization Geneva, 2021).

112   Hartley, S. *et al.* Ugandan stakeholder hopes and concerns about gene drive mosquitoes for malaria control: new directions for gene drive risk governance. *Malar J* **20**, 149, doi:10.1186/s12936-021-03682-6 (2021).

113   Annas, G. J. *et al.* A Code of Ethics for Gene Drive Research. *CRISPR J* **4**, 19-24, doi:10.1089/crispr.2020.0096 (2021).

114   Dubovskiy, I. M. *et al.* More than a colour change: insect melanism, disease resistance and fecundity. *Proc Biol Sci* **280**, 20130584, doi:10.1098/rspb.2013.0584 (2013).

115   Mustard, J. A., Beggs, K. T. & Mercer, A. R. Molecular biology of the invertebrate dopamine receptors. *Arch Insect Biochem Physiol* **59**, 103-117, doi:10.1002/arch.20065 (2005).

116   Rehr, S. S., Janzen, D. H. & Feeny, P. P. L-dopa in legume seeds: a chemical barrier to insect attack. *Science* **181**, 81-82, doi:10.1126/science.181.4094.81 (1973).

117   Giraldo, D. *et al.* Human scent guides mosquito thermotaxis and host selection under naturalistic conditions. *Curr Biol* **33**, 2367-2382 e2367, doi:10.1016/j.cub.2023.04.050 (2023).

118   Tripathi, A. K., Mlambo, G., Kanatani, S., Sinnis, P. & Dimopoulos, G. Plasmodium falciparum Gametocyte Culture and Mosquito Infection Through Artificial Membrane Feeding. *J Vis Exp*, doi:10.3791/61426 (2020).

119   Eisenman, H. C., Chow, S. K., Tse, K. K., McClelland, E. E. & Casadevall, A. The effect of L-DOPA on Cryptococcus neoformans growth and gene expression. *Virulence* **2**, 329-336, doi:10.4161/viru.2.4.16136 (2011).

120   Smith, D. F. Q. *et al.* Glyphosate inhibits melanization and increases susceptibility to infection in insects. *PLoS Biol* **19**, e3001182, doi:10.1371/journal.pbio.3001182 (2021).

121   Schindelin, J. *et al.* Fiji: an open-source platform for biological-image analysis. *Nat Methods* **9**, 676-682, doi:10.1038/nmeth.2019 (2012).

122   Fung, B. M., Khitrin, A. K. & Ermolaev, K. An improved broadband decoupling sequence for liquid crystals and solids. *J Magn Reson* **142**, 97-101, doi:10.1006/jmre.1999.1896 (2000).

123   Lehmann, P. F. & White, L. O. Chitin assay used to demonstrate renal localization and cortisone-enhanced growth of Aspergillus fumigatus mycelium in mice. *Infect Immun* **12**, 987-992, doi:10.1128/iai.12.5.987-992.1975 (1975).

124   Camacho, E. *et al.* N-acetylglucosamine affects Cryptococcus neoformans cell-wall composition and melanin architecture. *Microbiology (Reading)* **163**, 1540-1556, doi:10.1099/mic.0.000552 (2017).

125   Organization, W. H. *Test procedures for insecticide resistance monitoring in malaria vector mosquitoes*. 2nd ed. edn, (2018).

126   Jacobs, E. *et al.* Cuticular profiling of insecticide resistant Aedes aegypti. *Sci Rep* **13**, 10154, doi:10.1038/s41598-023-36926-3 (2023).

127   Matsumoto, H., Tanaka, K., Noguchi, H. & Hayakawa, Y. Cause of mortality in insects under severe stress. *Eur J Biochem* **270**, 3469-3476, doi:10.1046/j.1432-1033.2003.03745.x (2003).

Acknowledgments

Author contributions

E.C.: conceptualization, methodology, validation, formal analysis, investigation, project administration, funding acquisition, writing—original draft, writing-review and editing, visualization. Y.D., C.C., R.J.B.C., R.G.S., Y.A-R., D.F.Q.S., E.J., I.H., J.A.P-M., M.DP., A.D., A.J., B.S., G.M., A.T.: methodology, validation, formal analysis, investigation, writing— writing-review and editing, visualization. N.A.B.: Resources, writing-review, and editing. R.E.S.: Resources, supervision, writing-review and editing, and funding acquisition. D.G.: Resources, supervision, validation, writing-review, and editing. A.C.: conceptualization, supervision, project administration, resources, supervision, writing-review and editing, and funding acquisition.

Funding Acknowledgements

1

Figures

Fig 1. Experimental overview for investigating the impact of L-DOPA-supplemented sugar meal on *A. gambiae* mosquitoes. Created in BioRender. Camacho, E. (2025) https://BioRender.com/a17m623

Fig 2. Melanization pathways in insects. In *Anopheles* female mosquitoes, melanin synthesis relies mostly on dopamine produced from the blood meal-derived phenylalanine; however, other precursors from plant sources such as tyrosine or L-DOPA are used by both female and male mosquitoes for the generation of this biopolymer. Most melanins synthesized in insects derive from L-DOPA or dopamine in a reaction initiated by phenoloxidases present in the hemolymph; however, there is one possible minor pathway from a degradation product of dopamine: 3,4-dihydroxyphenylaldehide (DOPAL). DOPAL is a highly unstable compound that reacts with primary amines, leading to protein crosslinking and inactivation. Current literature suggests that its toxicity outweighs its benefits; evidence for DOPAL melanin formation in any biological system remains to be established. Simultaneously but via an independent pathway, dopamine serves as substrate for a process known as sclerotization which promotes hardening of insect cuticles (exoskeleton) and prevents desiccation, dehydration, and invasion by foreign organisms. This process is catalyzed by cuticle-bound phenoloxidases [12,17]. Created in BioRender. Camacho, E. (2025) https://BioRender.com/d90z642

Fig 3. L-DOPA supplementation exerts a hormesis effect. a Daily proportion of surviving mosquitoes after L-DOPA feeding in 1.5% sugar meal at various supplementation concentrations. Each survival curve represents pooled data from three independent experiments (n= 75). Survival curves for L-DOPA-fed mosquitoes were compared statistically to the survival curves of control mosquitoes using Log-rank Mantel-Cox tests; ns not significant, *p = 0.0113 0.6 mM, **p = 0.0007 0.2 mM, ****p < 0.0001 2 mM - 10 mM. **b** Cumulative survival percentage at days 4, 8 and 14 shows how mosquitoes adapt to the toxic effects of L-DOPA at concentrations below and above 1 mM over time. **c** Daily proportion of surviving mosquitoes after dopamine feeding in 1.5% sugar meal at various supplementation concentrations. Each survival curve represents pooled data from three independent experiments (n= 75). Survival curves for dopamine-fed mosquitoes were compared statistically to the survival curves of control mosquitoes using Log-rank Mantel-Cox tests; ns not significant, ****p < 0.0001 2 mM. **d** Cumulative survival percentage at days 4, 8 and

34

1   14 shows highly toxic effects of dopamine over time and striking death observations for sugar-fed

2   control mosquitoes.

3   **Fig 4. Comparative transcriptome analysis of *A. gambiae* gene expression for L-DOPA-fed**

4   **and sugar-fed female mosquitoes.** **a** Volcano plot of differentially expressed genes (DEGs) in

5   whole (headless) mosquitoes. Significantly upregulated and downregulated genes are highlighted

6   in red and blue spots, respectively. **b** DEGs by gene ontology category in whole L-DOPA-fed

7   female mosquitoes compared with sugar-fed (control) females. Differential gene expression was

8   considered significant when the expression fold change (L-DOPA-fed versus sugar-fed) was ≥1.3

9   on a -$\log_{10}$ scale (P < 0.05). Categories are R/S/M, oxidoreductive, stress-related, and

10   mitochondrial. **c** Volcano plot of differentially expressed genes (DEGs) in mosquito midguts.

11   Significantly upregulated and downregulated genes are highlighted in red and blue spots,

12   respectively. **d** DEGs by gene ontology category in midguts from L-DOPA-fed female mosquitoes

13   compared with sugar-fed females. Differential gene expression was considered significant when

14   the expression fold change (L-DOPA-fed versus sugar-fed) was ≥1.3 on a -$\log_{10}$ scale (P < 0.05).

15   Categories are R/T/T, replication, transcription, and translation; R/S/M, oxidoreductive, stress-

16   related, and mitochondrial.

17   **Fig 5. Differential transcript abundances of melanin-related physiological processes in *A.***

18   ***gambiae* female mosquitoes following feeding of a sugar-meal supplemented with 1 mM L-**

19   **DOPA for 4 d.** $\log_2$ scale indicates transcripts that were found at significantly higher (red) or

20   lower (blue) levels in whole (headless) mosquitoes (upper panel) and midguts (lower panel) from

21   *A. gambiae* post L-DOPA-feeding versus sugar-fed (controls). **a** Set of immune-related

22   transcripts. **b** Set of cuticle-related transcripts.

23   **Fig 6. L-DOPA exhibits antiparasitic and antifungal activity. a** *P. falciparum* infection intensity

24   and prevalence in adult female mosquitoes fed on a sugar meal supplemented with a L-DOPA or

25   dopamine concentrations. Each circle indicates the number of oocysts on an individual midgut;

26   horizontal bars represent the median value of oocysts. Each experiment consisted of three

27   biological replicates, and data were pooled to generate the graph. Statistical analysis of infection

28   intensity was performed using the Kruskal-Wallis test with Dunn's multiple comparisons post-test

29   against the control; ns not significant, left panel **p = 0.0081, right panel **p = 0.0019. Statistical

30   significance for prevalence of infection was assessed with a Fisher's exact test, ns. **b** *In vitro*

31   assessment of L-DOPA toxicity to sexual and asexual stages of *P. falciparu*m parasite. Use of L-

32   DOPA concentrations ranging from 0.25 mM to 2 mM during *in vitro* parasite culture, appeared

1 more toxic to asexual stages of the parasite than to sexual stages. Data from three biological

2 replicates were pooled to generate the graph. Data was analyzed with ordinary two-way ANOVA

3 with Dunnett's multiple comparisons tests against individual controls; ns not significant; ****$p <$

4 0.0001. **c** Fungal load in L-DOPA-fed female mosquitoes shows a reduction compared to control.

5 Each circle corresponds to a whole mosquito homogenate; bars represent the mean value of

6 fungal CFUs, and error bar corresponds to SD. Data from three biological replicates were pooled

7 to generate the graph. **d** Cryptococcal yeasts are successfully melanized in the abdomens of *A.*

8 *gambiae* female mosquitoes 24 h post-injection of *C. neoformans* H99-GFP strain (1 x 10^8

9 yeasts/ml). Live yeast cells (green arrows), Dead yeast cells (white arrows). Representative

10 images from abdomen sections of 10 female mosquitoes at two independent experiments. **e** qRT-

11 PCR analysis of mRNA abundance in whole mosquitoes from key genes [dopa decarboxylase

12 (DDC), gambicin (GAM), phenoloxidase 1 (PPO1), and leucine-rich immunomodulator 15

13 (LRIM15)] involved in the mosquito melanization pathway and *Plasmodium* parasite development.

14 Data represent the mean ± SE of three or more independent replicates, analyzed using unpaired

15 one-way ANOVA with Holm-Sidák's multiple comparison test to determine gene expression

16 relative to housekeeping S7 gene; ns not significant, **$p = 0.0041$, *$p = 0.0235$.

17 **Fig 7. Oral L-DOPA boosts mosquito cuticular melanization via a non-canonical pathway.**

18 **a** Dietary L-DOPA enhances cuticle pigmentation of *A. gambiae* female mosquitoes in a dose-

19 dependent manner. *Upper panel*, Representative images of *A. gambiae* female mosquitoes fed

20 with a sugar meal supplemented with different concentrations of L-DOPA for up to 14 d. Scale

21 bar, 1 mm; *Lower panel*, Quantification of cuticle darkening at 8 and 14 d. Each dot corresponds

22 to an individual mosquito. Mean with 95% CI from 2-3 biological replicates are shown in graphs.

23 Statistical significance was determined by Left panel, unpaired two-tailed *t*-test, *$p = 0.0342$; and

24 Right panel, ordinary one-way analysis of variance (ANOVA) with Dunnett's multiple comparison

25 test against control, ns not significant, *$p = 0.0365$, ****$p < 0.0001$). **b** *Top panel,* TEM micrographs

26 exhibiting distinct electron-dense bands within the endocuticle of L-DOPA-fed mosquitoes that

27 are not seen in the control. Scale bar, 500 nm. *Lower panel,* Measurements of cuticular thickness

28 from legs of female mosquitoes fed with L-DOPA supplemented sugar meals and control show

29 increased values for exo and endocuticle. Two-way ANOVA with Tukey's multiple comparisons

30 test; ****$p < 0.0001$. Data represent measurements from 10 femurs per condition with 3-5

31 representative images analyzed per female. A minimum of 3 total cuticle and endocuticle

32 measurements were taken per image. Means with SD are shown on the graph. **c** L-DOPA

33 supplementation augments content of indole groups. *Left panel*, DPMAS ^{13}C ssNMR spectra of

1 ^{13}C-L-DOPA fed mosquitoes display pigment peaks (green arrows) with greater relative intensities

2 than their respective controls. Spectra were normalized to the tallest peak (lipid peak at ~30 ppm);

3 Right panel, CPMAS ^{13}C ssNMR spectra of ^{13}C-L-DOPA fed mosquitoes corroborate the assertion

4 that ^{13}C-L-DOPA has been nearly-exclusively used to make melanin instead of being broken down

5 and used as a nutrient source. Spectra were normalized to the tallest peak (polysaccharide peak

6 at ~72 ppm). Representative data from 2 biological replicates. **d** Quantification of chitin content in

7 whole *A. gambiae* female mosquitoes demonstrates no significant differences between sugar-fed

8 (control) and L-DOPA-fed mosquitoes. Data correspond to 3 biological replicates. Mean with SD.

9 Two-tailed unpaired, nonparametric Mann-Whitney test; ns not significant. **e** EPR spectroscopy

10 analysis of acid-resistant material isolated from *An. gambiae* and *Ae. aegypti* yellow mutant strain

11 L-DOPA-fed (red spectra) and sugar-fed (blue spectra). Representative data from 2 biological

12 replicates. Fungal eumelanin was used as positive control (black spectrum).

13 **Fig. 8. Dietary L-DOPA darkening of cuticle increases heat-exposed mosquito**

14 **temperatures following light exposure and decreases lifespan. A)** *A. gambiae* female

15 mosquitoes fed with a sugar meal supplemented with different concentrations of L-DOPA (0.2

16 mM to 1 mM) for 8 d displayed a dose-dependent ability to absorb heat. **B)** Exposure to a direct

17 light source during 1 min (shadowed area) demonstrated that 1mM L-DOPA- fed mosquitoes (red

18 squares) exhibited a warmer body temperature than sugar-fed control (blue circles). Post-

19 irradiation when light is turned off (unshadow area), L-DOPA-fed mosquitoes (red squares) were

20 distinctly hotter than sugar-fed controls (blue circles), starting to cool down but kept warmer than

21 control The thermograph was obtained using the Teledyne FLIR E95 camera, and the

22 temperature of each mosquito was extracted using the FLIR software, which provided the

23 maximum, minimum, and average temperatures within a box selection for each mosquito. The

24 maximum temperature for each mosquito was used to generate the graph, which represents the

25 average (+/- Standard Deviation) of the six maximum temperatures corresponding to the two

26 experimental groups (control sugar-fed and 1 mM L-DOPA-fed). Mann-Whitney test, p = 0.0173.

27 Mann-Whitney test, *p = 0.0173. **C)** Lifespan of mosquitoes maintained on 1.5% sugar with 1 mM

28 L-DOPA was diminished in comparison to sugar-only fed mosquitoes. Representative data from

29 3 biological replicates. **D)** Number of eggs laid by female mosquitoes after feeding with a sugar

30 meal supplemented with 1 mM L-DOPA during 4 d before a blood meal on mice. Mann-Whitney

31 test, NS, not significant, p = 0.1987. Red lines denote mean. **E)** Hatching rate at 27 °C indicating

32 average percentage of eggs giving rise to 1st and 2nd instar larvae. Mann-Whitney test, NS, not

33 significant. p = 0.9390. Red lines denote mean.

1 **Fig. 9 Dietary L-DOPA metabolism and probing for dopaminergic bacteria amongst gut**

2 **microbiota from field-caught mosquitoes.** **A)** Quantification of dopamine by HPLC from whole

3 *Anopheles* mosquitoes post 4 d of dietary L-DOPA suggests tight regulation of L-DOPA

4 conversion into dopamine. Data correspond to 2 independent biological replicates from 5-pooled

5 mosquitoes per condition. A 2-way analysis of variance (ANOVA) with Tukey's multiple

6 comparisons test showed no significant differences among and between groups. **B)** Plate

7 confrontational assays showed induced fungal melanization due to melanin precursors released

8 by bacterial isolates. A) *Comamonas* sp.; B) *Enterococcus hormaechei*; C) *Aeromonas*

9 *hydrophila*; D) *Serratia marcescens* E) *Chromobacterium subtsugae* ΔvioS F) *Enterococcus* sp.

10 *Cryptococcus* strains (top: *C. gattii* WM179; middle: *C. neoformans* ΔLAC1; bottom: *C.*

11 *neoformans* H99) were streaked perpendicular to bacterial isolates in SM plates. The plates were

12 incubated at 30°C for 5-7 days. Images are representative of 3 biological replicates.

13 **Fig. 10 Alternative pathway for L-DOPA incorporation to the melanin synthesis in**

14 **mosquitoes. A)** L-DOPA serves as a substrate for cuticular melanization via DOPAL synthase

15 as a detoxification mechanism given a cellular redox environment that promotes L-DOPA

16 antioxidant properties (neutral or acid pH) [66], therefore preventing its conversion to dopamine via

17 a dopa decarboxylase. L-DOPA conversion into DOPAL leads into DOPAL buildup that promotes

18 oligomerization and quinone adduct formation ("quinonization") inhibiting its own metabolism and

19 the activity of other enzymes involved in the melanin biosynthesis such as dopa decarboxylase

20 (DDC), phenoloxidase 5 (PPO5), and dopachrome conversion enzyme (DCE)[65]. **B)** Model for

21 dietary L-DOPA-mediated cuticular melanization proposes that *Anopheles gambiae* female

22 mosquitoes use L-DOPA supplement in the sugar meal as a substrate for synthesizing cuticular

23 melanin. L-DOPA is internalized into the midgut epithelium and exported to the hemolymph by

24 sharing the same transporters with amino acids such as Na^+-driven amino acid transporter, alpha2

25 transporter, and/or SLC protein. Within regions of flexible cuticle, in the presence of DOPAL

26 synthase, L-DOPA is turned into DOPAL and H_2O_2 promoting oxidation of DOPAL catechol ring

27 that results in the formation of a melanized and protective flexible cuticle via crosslinking to

28 cuticular proteins[63,64]. The contribution of gut microbiota as well as from hemocytes as key

29 regulators of mosquito vectorial capacity and immunity, post a L-DOPA diet is under investigation.

30 Created in BioRender. Camacho, E. (2025) https://BioRender.com/d90z642

31 **Supplementary Data 1. Differentially Expressed Genes between 1mM L-DOPA-fed and**

32 **sucrose-fed *A. gambiae* female mosquitoes.** 10.6084/m9.figshare.27122907

1 **Supplementary Data 2.** DESeq2 Median Ratio normalization for 902 differentially expressed

2 genes in *A. gambiae* whole female mosquito post dietary L-DOPA.

3 10.6084/m9.figshare.28063112

4 **Supplementary Table 1.** Detection of melanin precursors released by diverse bacterial species.

5 **Supplementary Fig 1. Partek Flow analysis. A)** Principal component analysis (PCA) of 4 L-

6 DOPA-fed mosquito groups and 3 sugar-fed controls. Blue spheres represent control replicates;

7 red spheres represent L-DOPA-fed replicates. **B)** Top 20 KEGG Pathway enrichment analysis of

8 transcriptional data.

9 **Supplementary Fig 2.** qRT-PCR analysis of mRNA abundance in whole mosquitoes from critical

10 genes related to this study [phenoloxidase 5 (PPO5), 3,4-dihydroxyphenylacetaldehyde (DOPAL)

11 synthase, thioester-containing protein 1 (TEP1), propionyl-CoA synthetase (ProCoA). Data

12 represent the mean ± SE of three or more independent replicates, analyzed using unpaired by

13 one-way ANOVA and multiple comparison test to determine gene expression relative to

14 housekeeping S7 gene. NS, not significant

15 **Supplementary Fig 3. L-DOPA supplementation also enhances cuticular melanization in**

16 ***Anopheles gambiae* male mosquitoes. A)** ^{13}C DPMAS NMR spectra of ^{13}C-L-DOPA fed

17 mosquitoes display pigment peaks (green arrows) with greater relative intensities than their

18 controls. Spectra were normalized to the tallest peak (lipid peak at ~30 ppm). **B)** *Top panel,* TEM

19 micrographs displaying distinct electron-dense bands within the endocuticle of L-DOPA-fed

20 mosquitoes not seen in those of control. Scale bar, 500 nm. *Lower panel,* Measurements of

21 cuticular thickness from legs of male mosquitoes fed with a 1 mM L-DOPA supplemented sugar

22 meal show reduced exocuticle in comparison to controls (sugar-fed). NS, not significant; ****$p <$

23 0.0001; Two-way analysis of variance (ANOVA) with Tukey's multiple comparisons test.

24 **Supplementary Fig 4. Mapping white LED intensity distribution on the cooling block and**

25 **mosquitoes' temperature variance. A)** Apparent temperature of group of 20 mosquitoes fed

26 with up to 1 mM L-DOPA demonstrated that 1 mM L-DOPA-fed mosquitoes exhibited a warmer

27 temperature than sugar-fed controls (Trial 1). **B)** Apparent temperature of group of 20 mosquitoes

28 fed with 1 mM L-DOPA consistently demonstrated that 1 mM L-DOPA-fed mosquitoes exhibited

29 a warmer temperature that sugar-fed controls (Trial 2). **C)** Apparent temperature of individual

30 mosquitoes (n = 6) fed with 1 mM L-DOPA consistently demonstrated that 1 mM L-DOPA-fed

31 mosquitoes exhibited a warmer temperature that sugar-fed controls (Trial 3). **D)** Light intensity

1   (LUX) distribution on sample platform showing that luminous flux decreases around the edge of

2   the cooling block.

3   **Supplementary Fig 5. Gut microbiota can secrete dopamine.** Chromatographs of cell-free

4   bacterial supernatants after growth for 24, 48, 72 and 96 h Luria Bertani media at 30ºC.

5   Overlapped dotted chromatograph corresponds to 1 mM spike dopamine. Red arrows show

6   points at which samples were collected. The elution time was measured in minutes and the

7   absorbance is measured at 214 nm in arbitrary units. For Fast Protein Liquid Chromatography

8   (FPLC), we used a C18 Reverse-Phase column to observe the dopamine peaks. 25 mM

9   Potassium Phosphate buffer (pH 3.1) was used as an isocratic mobile phase at a flow rate of 1

10   ml/min.

11   **Supplementary Fig 6. L-DOPA-sucrose solutions pH monitored over time.** Measurement of

12   pH from sucrose solution while incubated at 27°C inside the mosquito chamber displays

13   progressive acidification. Supplementation with L-DOPA accentuates this trend. Data

14   corresponding to three independent measurements for all conditions. Bars correspond to mean

15   with 95% confidence interval. Statistical analyses were performed using a Two-way analysis of
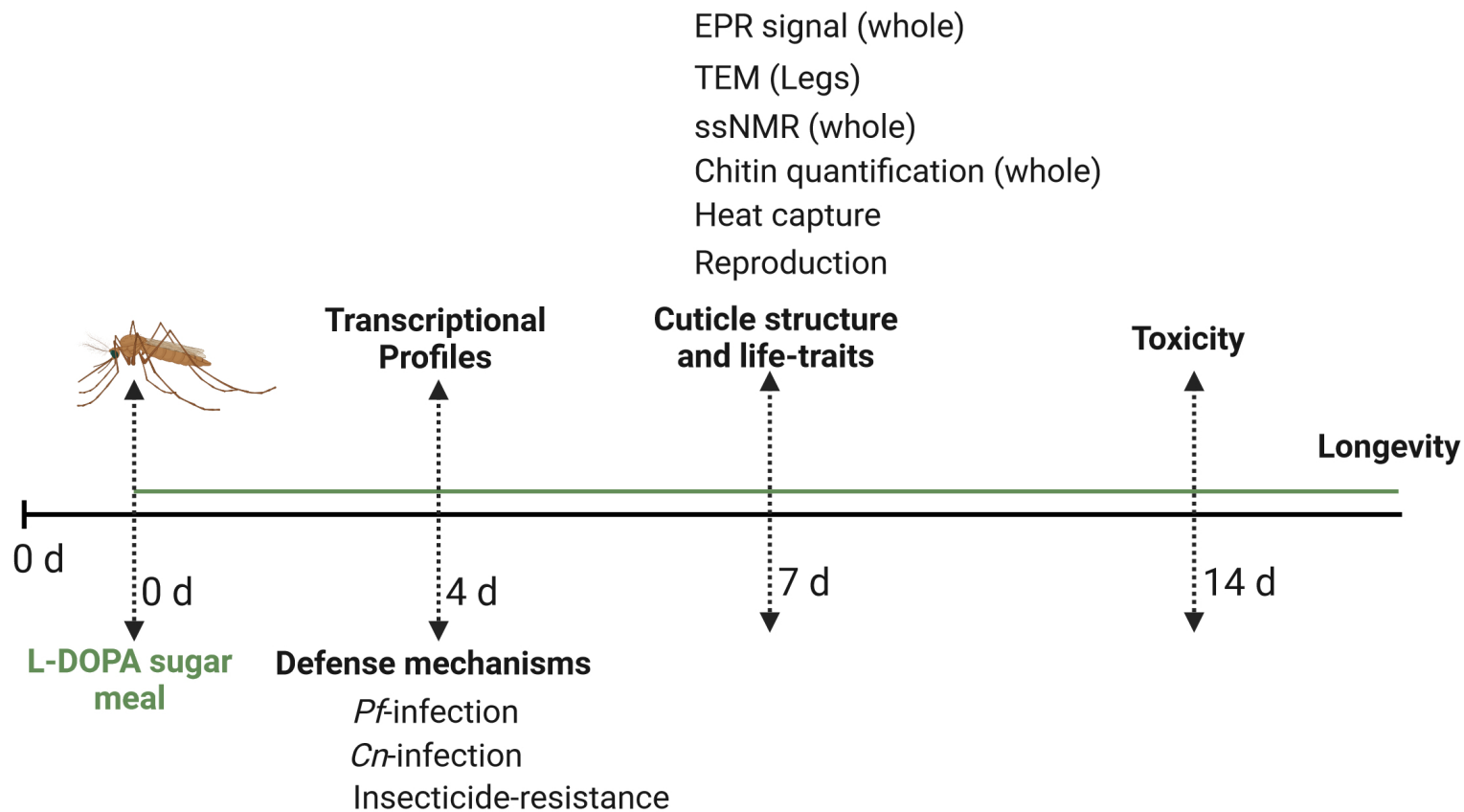
16   variance (ANOVA) with Sidak's multiple comparisons test.

17

Fig 1. Experimental overview for investigating the impact of L-DOPA-supplemented sugar meal on *A. gambiae* mosquitoes.
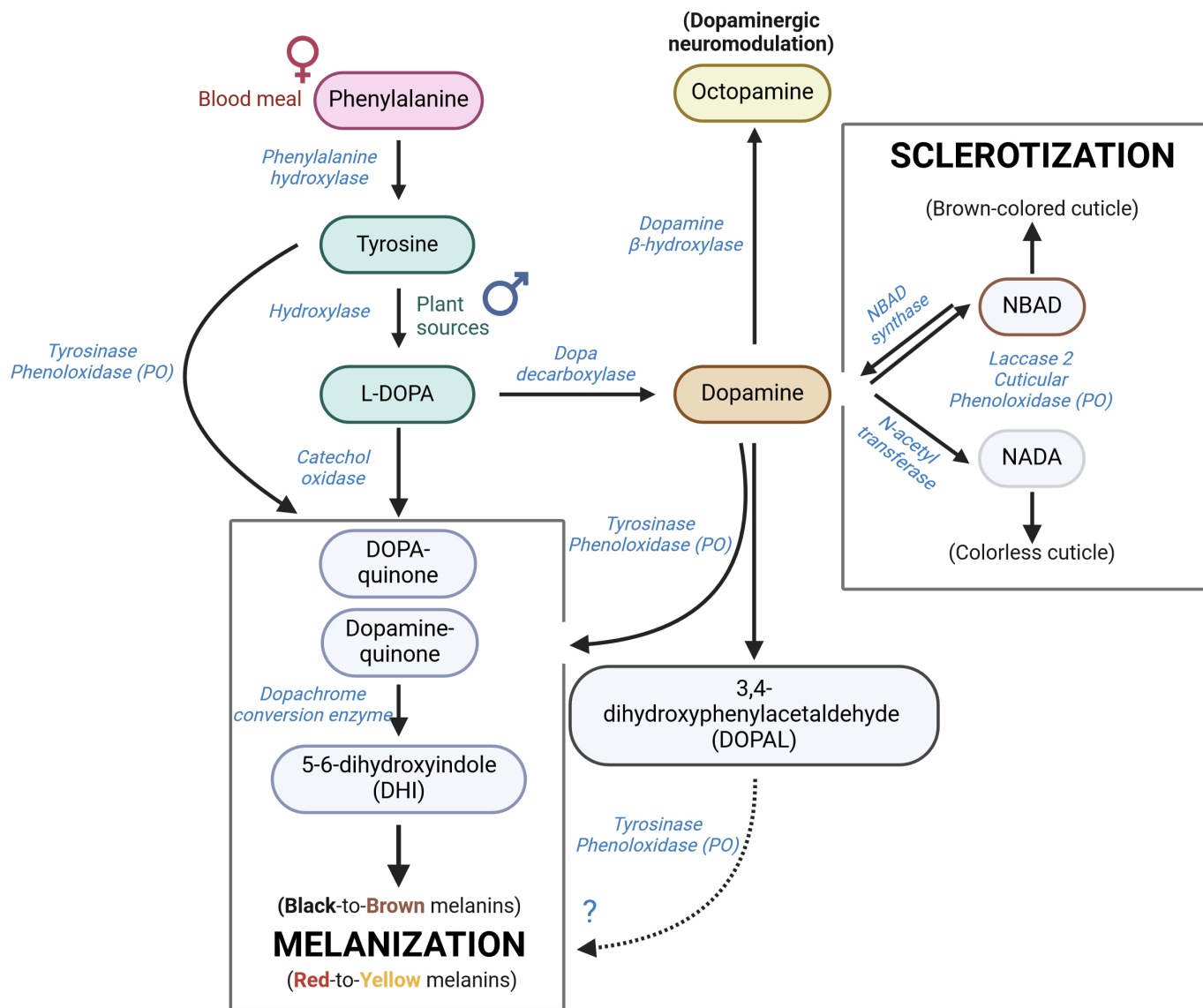
Fig 2. Melanization pathways in insects. In *Anopheles* female mosquitoes, melanin synthesis mostly depends on dopamine produced from the blood meal-derived phenylalanine; however, other precursors from plant sources such as tyrosine or L-DOPA are used by both female and male mosquitoes for the generation of this biopolymer. Most melanins synthesized in insects derive from L-DOPA or dopamine in a reaction initiated by phenoloxidases present in the hemolymph; however, there is one possible minor pathway from a degradation product of dopamine: 3,4-dihydroxyphenylacetaldehyde (DOPAL). DOPAL is a highly unstable compound that reacts with primary amines, leading to protein crosslinking and inactivation. Current literature suggests that its toxicity outweighs its benefits, thus evidence of DOPAL melanin formation in any biological system remains to be determined. Simultaneously but via an independent pathway, dopamine serves as substrate for a process known as sclerotization which promotes hardening of insect cuticles (exoskeleton) and prevents desiccation, dehydration, and invasion from foreign organisms. This process is catalyzed by cuticle-bound phenoloxidases [12,17]. Figure created with Biorender.com
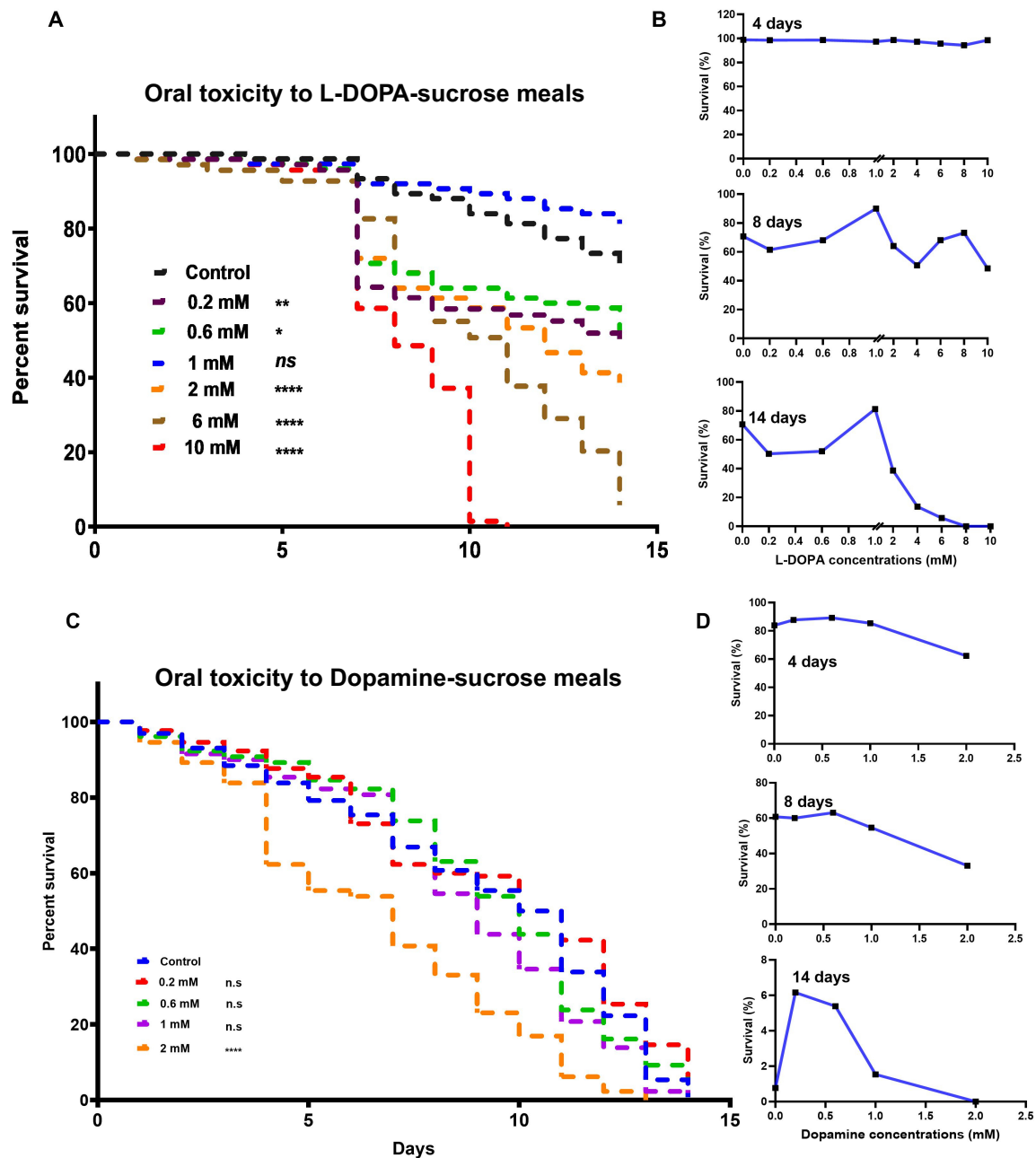
Fig 3. L-DOPA supplementation exerts a hormesis effect. A) Daily proportion of surviving mosquitoes after L-DOPA feeding in 1.5% sugar meal at various concentrations. Each survival curve represents pooled data from three independent experiments (n= 75). Survival curves for L-DOPA-fed mosquitoes were compared statistically to the survival curves of control mosquitoes using Log-rank Mantel-Cox tests (NS, not significant, *p = 0.0113, **p = 0.0040, ****p < 0.0001). **B)** Cumulative survival percentage at days 4, 8 and 14 shows how mosquitoes adapt to toxic effects of L-DOPA at concentrations below and above 1 mM over time. **C)** Daily proportion of surviving mosquitoes after dopamine feeding in 1.5% sugar meal at various concentrations. Each survival curve represents pooled data from three independent experiments (n= 75). Survival curves for dopamine-fed mosquitoes were compared statistically to the survival curves of control mosquitoes using Log-rank Mantel-Cox tests (NS, not significant, ****p < 0.0001). **D)** Cumulative survival percentage at days 4, 8 and 14 shows highly toxic effects of dopamine over time and striking death on sugar-fed control mosquitoes.
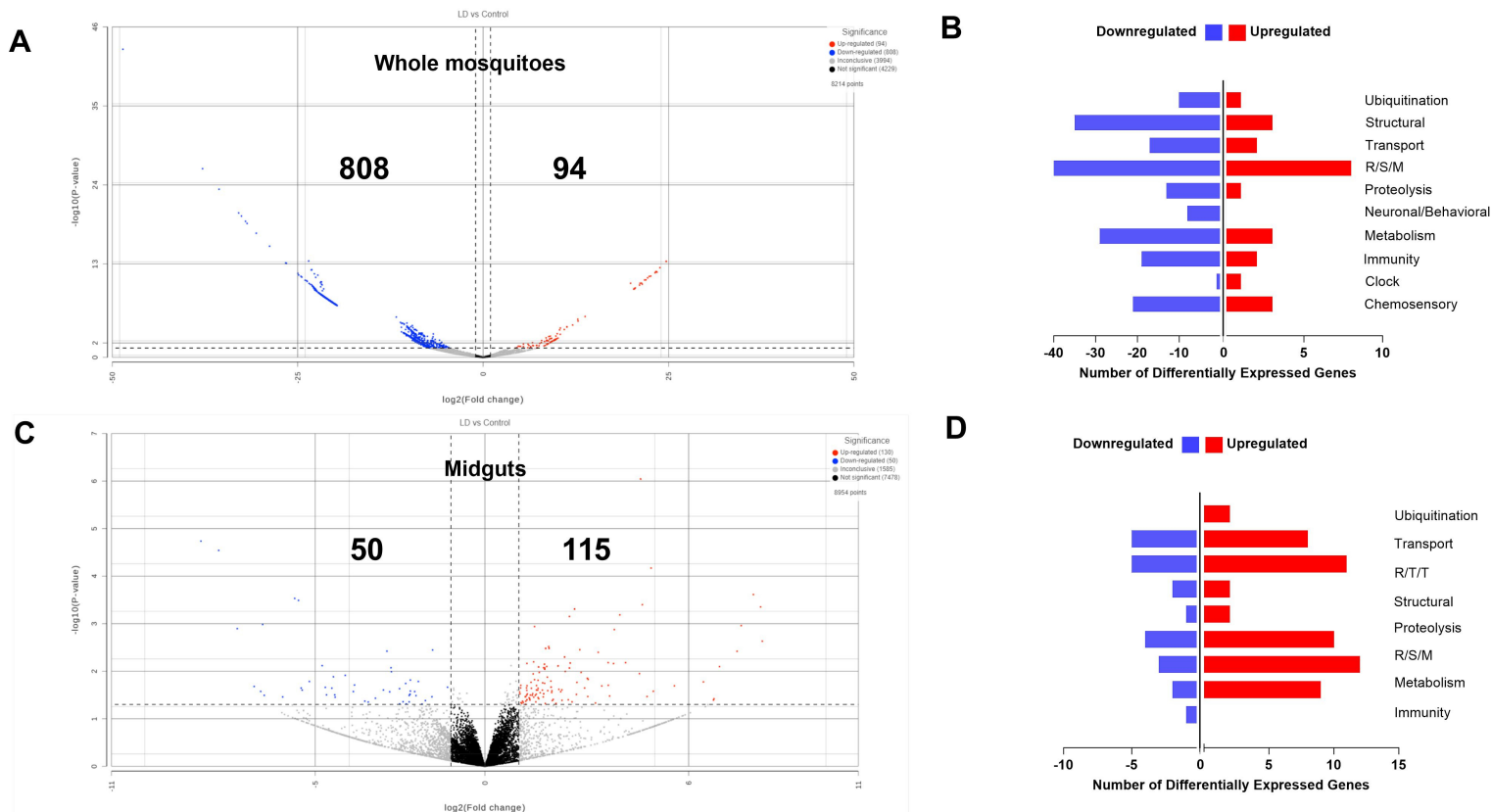
Fig 4. Comparative transcriptome analysis of *A. gambiae* gene expression between L-DOPA-fed and sugar-fed female mosquitoes.
A) Volcano plot of differentially expressed genes (DEGs) in whole (headless) mosquitoes. Significantly upregulated and downregulated genes are highlighted in red and blue spots, respectively. **B)** DEGs by gene ontology category using VectorBase in whole L-DOPA-fed female mosquitoes compared with sugar-fed (control) females. Differential gene expression was considered significant when the expression fold change (L-DOPA-fed versus sugar-fed) was ≥1.3 on a -$\log_{10}$ scale (P < 0.05). R/S/M, oxidoreductive, stress-related, and mitochondrial **C)** Volcano plot of differentially expressed genes (DEGs) in mosquito midguts. Significantly upregulated and downregulated genes are highlighted in red and blue spots, respectively. **D)** DEGs by gene ontology category in midguts from L-DOPA-fed female mosquitoes compared with sugar-fed females. Differential gene expression was considered significant when the expression fold change (L-DOPA-fed versus sugar-fed) was ≥1.3 on a -$\log_{10}$ scale (P < 0.05). R/T/T, replication, transcription, and translation; R/S/M, oxidoreductive, stress-related, and mitochondrial.

A

IMMUNE-RELATED

WHOLE MOSQUITOES

Gene ID	Log2 Fold Change	Gene name	P-value
AGAP005799	4.63	Dally protein	4.29E-14
AGAP009091	-2.37	Aromatic-L-amino-acid decarboxylase (DDC)	4.10E-02
AGAP007627	-2.37	Nitric oxide synthase protein (NOS)	4.05E-02
AGAP000536	-2.44	Peptidoglycan recognition protein (short) (PGRP-S1)	3.47E-02
AGAP012326	-2.77	TOLL-like receptor 7 (TOLL7)	1.98E-02
AGAP004806	-2.79	Galectin 6 (GAL6)	1.47E-02
AGAP012932	-2.81	Autophagy-related protein 9	3.03E-02
AGAP012616	-2.88	prophenoloxidase 5 (PPO5)	2.41E-02
AGAP010833	-2.88	CLIP-domain serine protease (CLIPB14)	3.97E-02
AGAP010485	-2.92	Dopamine beta-monooxygenase (DBH)	1.08E-02
AGAP002451	-4.32	Class B Scavenger Receptor (SCRB1)	3.54E-08
AGAP002815	-4.35	CLIP-domain serine protease (CLIPA15)	1.83E-08
AGAP005959	-4.40	Dopachrome-conversion enzyme (DCE)	6.55E-09
AGAP007692	-4.43	Serine Protease Inhibitor (SRPN14)	2.96E-10
AGAP011952	-4.47	Short caspase 3 (CASPS3)	1.17E-09
AGAP007410	-4.50	C-type lectine mannose binding (CTLMA5)	4.68E-10
AGAP011693	-4.54	Long caspase (CASPL1)	6.92E-11

MIDGUTS

Gene ID	Log2 Fold Change	Gene name	P-value
AGAP005583	2.31	Phosphoinositide-3-kinase, regulatory subunit (PPI3K)	1.97E-02
AGAP010817	2.19	CUB domain-containing protein, predicted peroxidase	1.12E-02
AGAP004148	1.86	CLIP domain-containing serine protease (CLIPB5)	2.64E-02
AGAP011360	0.42	Kurtz arrestin-like protein (ARRK)	3.17E-02
AGAP011792	-2.15	CLIP domain-containing serine protease (CLIPA7)	3.15E-02

B

CUTICLE-RELATED

WHOLE MOSQUITOES

Gene ID	Log2 Fold Change	Gene name	P-value
AGAP004270	3.25	Hexosaminidase D	4.67E-03
AGAP009191	3.21	Glutathione S-transferase epsilon class 6 (GSTE6)	6.01E-03
AGAP013219	-2.86	Elongase, elongation of very long chain fatty acids protein 7 (ELO7)	3.46E-02
AGAP005371	-2.88	Carboxylesterase beta esterase (COEBE2C)	4.33E-02
AGAP005512	-2.90	Elongase, Elongation of very long chain fatty acids protein (ELO4)	3.48E-02
AGAP011936	-3.04	Serpentine (chitin deacetylase)	1.36E-02
AGAP001473	-3.05	Propionyl-CoA synthetase (ProCoA)	4.18E-04
AGAP009195	-3.12	Glutathione S-transferase epsilon class 1 (GSTE1)	6.89E-03
AGAP004784	-3.15	Fatty acyl-CoA reductase 2	2.16E-03
AGAP001748	-3.33	Chitin synthase 1 (CHS1A,B)	2.80E-04
AGAP000820	-4.32	Cuticular protein RR-1 (CPR125)	3.97E-08
AGAP005511	-4.36	Elongation of very long chain fatty acids protein 2 (ELO2)	1.47E-08
AGAP009241	-4.41	Cytochrome P450 (CYP4C36)	4.65E-09
AGAP007980	-4.44	Cuticular protein CPCFC family (CPCFC1)	2.25E-09
AGAP000986	-4.47	Cuticular protein (CPAP3-D)	1.14E-09
AGAP013120	-4.57	Chitinase (CHT5-5)	2.13E-11
AGAP006049	-4.64	Cytochrome P450 (CYP4J10)	3.48E-12

MIDGUTS

Gene ID	Log2 Fold Change	Gene name	P-value
AGAP008685	2.29	Juvenile hormone epoxide hydrolase 2 (Jheh2)	6.75E-05
AGAP005660	-1.78	Cytochrome P450 (CYP305A4)	4.46E-02
AGAP009246	-2.70	Cytochrome P450 (CYP4C27)	3.21E-02
AGAP010362	-2.77	Chitin binding domain-containing protein	2.09E-02

Fig 5. Differential transcripts abundances of melanin-related physiological processes in *A. gambiae* female mosquitoes following feeding of a sugar-meal supplemented with 1 mM L-DOPA for 4 d. Log_2 scale indicates transcripts that were found at significantly higher (red) or lower (blue) levels in whole (headless) mosquitoes (upper panel) and midguts (lower panel) from *A. gambiae* post L-DOPA-feeding versus sugar-fed (controls). **A)** Set of immune-related transcripts. **B)** Set of cuticle-related transcripts.
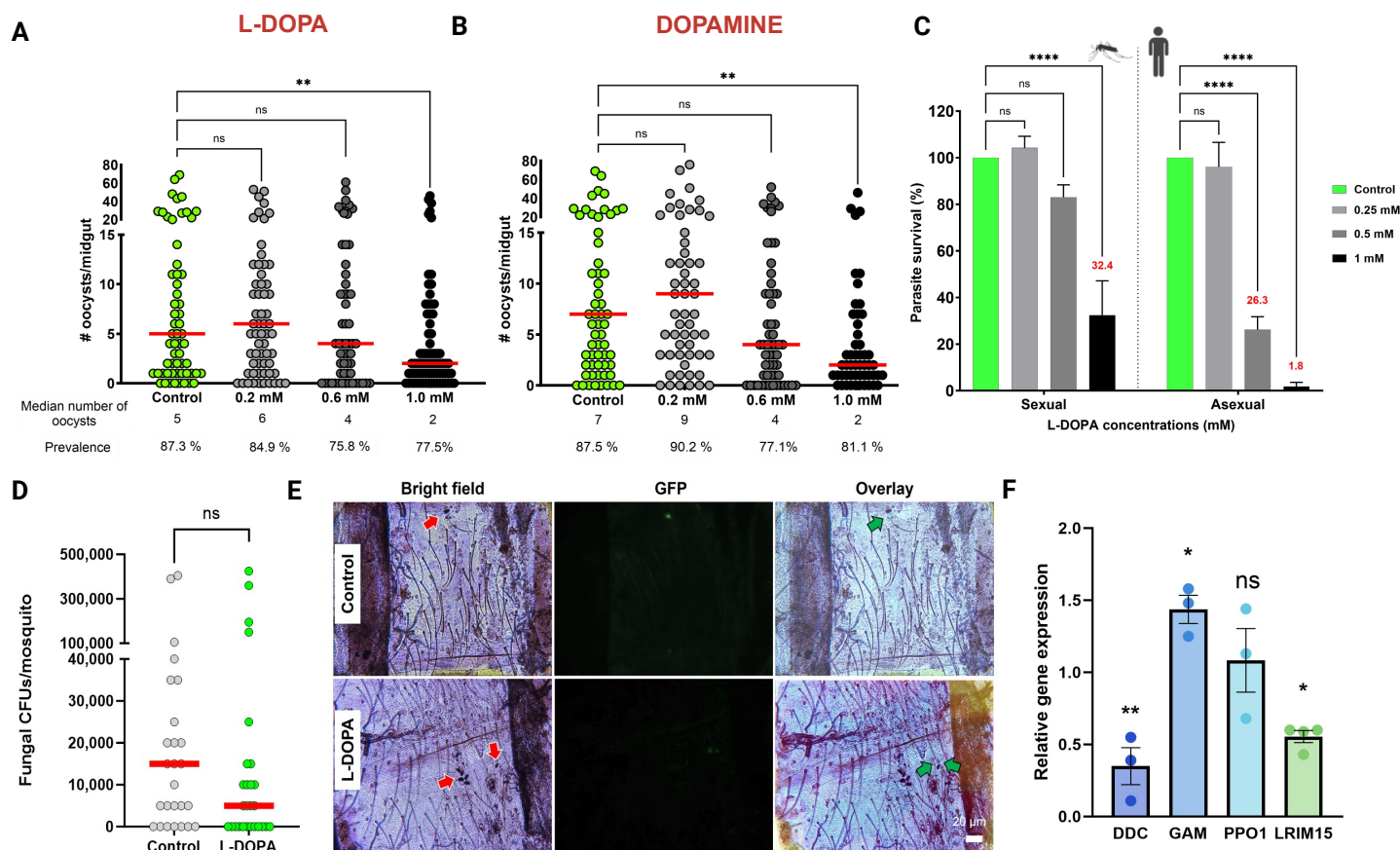
Fig 6. L-DOPA exhibits antiparasitic and antifungal activity. A) Intensity of *P. falciparum* oocyst load according to L-DOPA concentration in adult female mosquitoes. Each circle indicates the number of oocysts on an individual midgut; horizontal bars represent the median value of oocysts. n=3, NS, not significant, **p = 0.0081, One-way analysis of variance (ANOVA) nonparametric Kluskal-Wallis test. Statistical significance for Prevalence of infection was assessed with a Fisher's exact test, ns. **B)** Intensity of *P. falciparum* infection according to dopamine concentration in adult female mosquitoes. n=3, NS, not significant, **p = 0.0019, One-way ANOVA nonparametric Kluskal-Wallis test. Statistical significance for Prevalence of infection was assessed with a Fisher's exact test, ns. **C)** *In vitro* assessment of L-DOPA toxicity to sexual and asexual stages of *P. falciparum* parasite. Use of L-DOPA concentrations ranging from 0.25 mM to 2 mM during in vitro parasite culture, appeared more toxic to asexual stages of the parasite than to sexual stages. n=3, NS, not significant, ****$p <$ 0.0001, Two-way ANOVA with Dunnett's multiple comparisons tests against individual controls.   **D)** Fungal load in L-DOPA-fed female mosquitoes shows a reduction comparison to control. Each circle corresponds to a whole mosquito homogenate; horizontal red bars represent the median value of fungal CFUs. n=2, NS, not significant, Unpaired nonparametric Mann-Whitney test. **E)** Cryptococcal yeasts are successfully melanized (red arrow) in the abdomens of *A. gambiae* female mosquitoes 24 h post injection of *C. neoformans* H99-GFP strain (1 x 10⁷ yeasts/ml). Live yeast cells (green arrows), Dead yeast cells (red arrows). **F)** qRT-PCR analysis of mRNA abundance in whole mosquitoes from key genes [dopa decarboxylase (DDC), gambicin (GAM), phenoloxidase 1 (PPO1), and leucine-rich immunomodulator 15 (LRIM15)] involved in the mosquito melanization pathway and *Plasmodium* parasite development. Data represent the mean ± SE of three or more independent replicates, analyzed using unpaired by one-way ANOVA and multiple comparison test to determine gene expression relative to housekeeping S7 gene. NS, not significant, **p = 0.0041, *p = 0.0235.
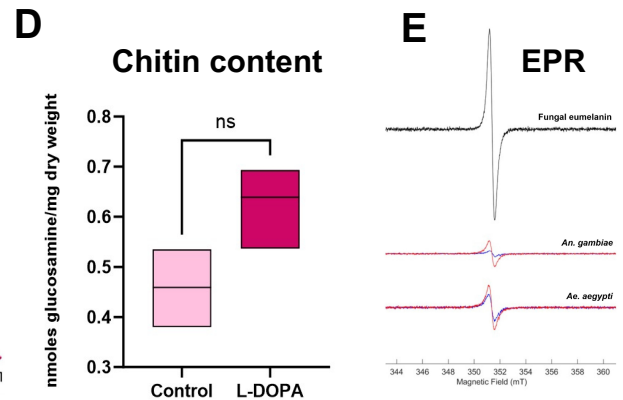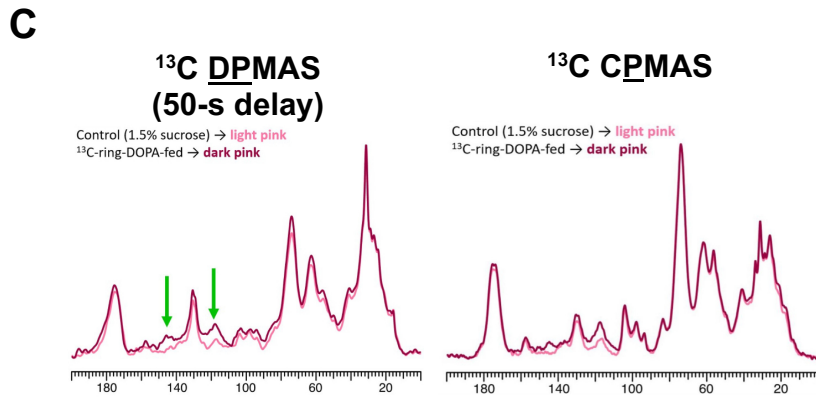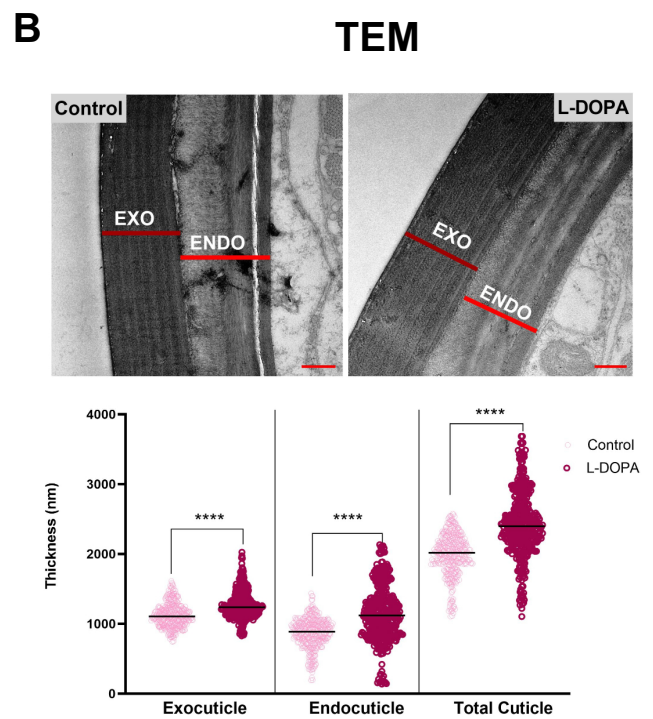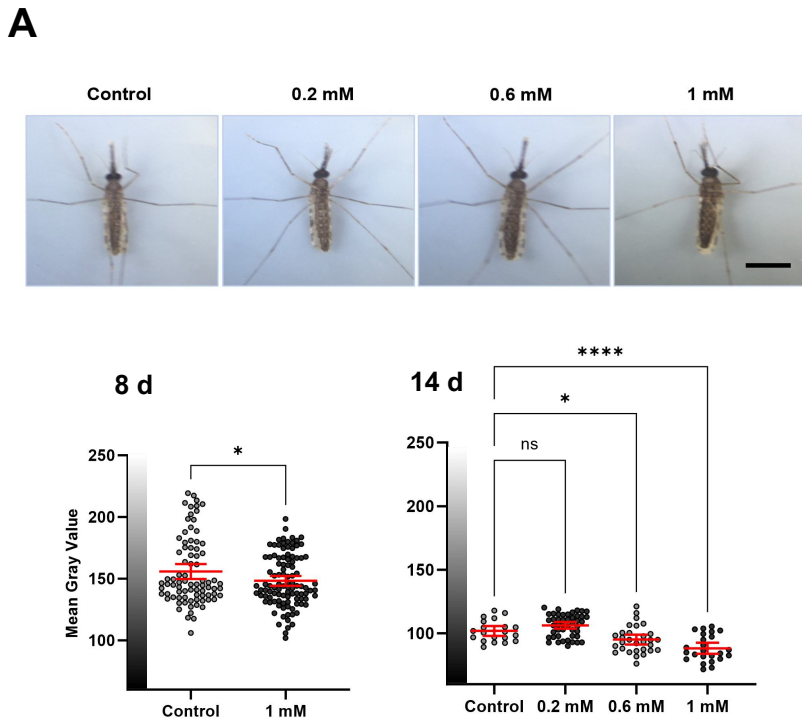
Fig 7. Oral L-DOPA boosts mosquito cuticular melanization via a non-canonical pathway. A) Dietary L-DOPA enhances cuticle pigmentation of *A. gambiae* female mosquitoes in a dose-dependent manner. *Upper panel*, Representative images of *A. gambiae* female mosquitoes fed with a sugar meal supplemented with different concentrations of L-DOPA for up to 14 d. Scale bar, 1 mm; *Lower panel*, Quantification of cuticle darkening at 8 and 14 d. Each dot corresponds to an individual mosquito. Data representative from 2-3 biological replicates. Statistical significance was determined by an Unpaired two-tailed t test with two or more data sets (Left panel, *p = 0.0342; Right panel, ns = not significant, *p = 0.0189, ****p < 0.0001) **B)** *Top panel,* TEM micrographs exhibiting distinct electron-dense bands within the endocuticle of L-DOPA-fed mosquitoes not seen in the control. Scale bar, 500 nm. *Lower panel,* Measurements of cuticular thickness from legs of female mosquito fed with L-DOPA supplemented sugar meals and control show increased exo and endocuticle. Bar corresponds to mean with SD. Two-way analysis of variance (ANOVA) with Sidak's multiple comparisons test. ****p<0.0001. **C)** L-DOPA supplementation augments content of indole groups. *Left panel*, DPMAS ^{13}C ssNMR spectra of ^{13}C-L DOPA fed mosquitoes display pigment peaks (green arrows) with greater relative intensities in comparison to their respective controls. Spectra were normalized to tallest peak (lipid peak at ~30 ppm); Right panel, CPMAS ^{13}C ssNMR spectra of ^{13}C-L-DOPA fed mosquitoes corroborate the assertion that ^{13}C-L-DOPA has been nearly-exclusively used to make melanin instead of being broken down and used as a nutrient source. Spectra were normalized to tallest peak (polysaccharide peak at ~75 ppm). Data are representative from 2 biological replicates. **D)** Quantification of chitin content in whole *A. gambiae* female mosquitoes exhibits demonstrate no significant differences between sugar-fed (control) and L-DOPA-fed mosquitoes. Data correspond to 3 biological replicates. Floating bars (min to max) Line at mean. NS, not significant; Unpaired, nonparametric Mann-Whitney test. **E)** EPR spectroscopy analysis of acid-resistant material isolated from *An. gambiae* and *Ae. aegypti* yellow mutant strain L-DOPA-fed (red spectra) and sugar-fed (blue spectra). Fungal eumelanin was used as positive control (black spectrum).
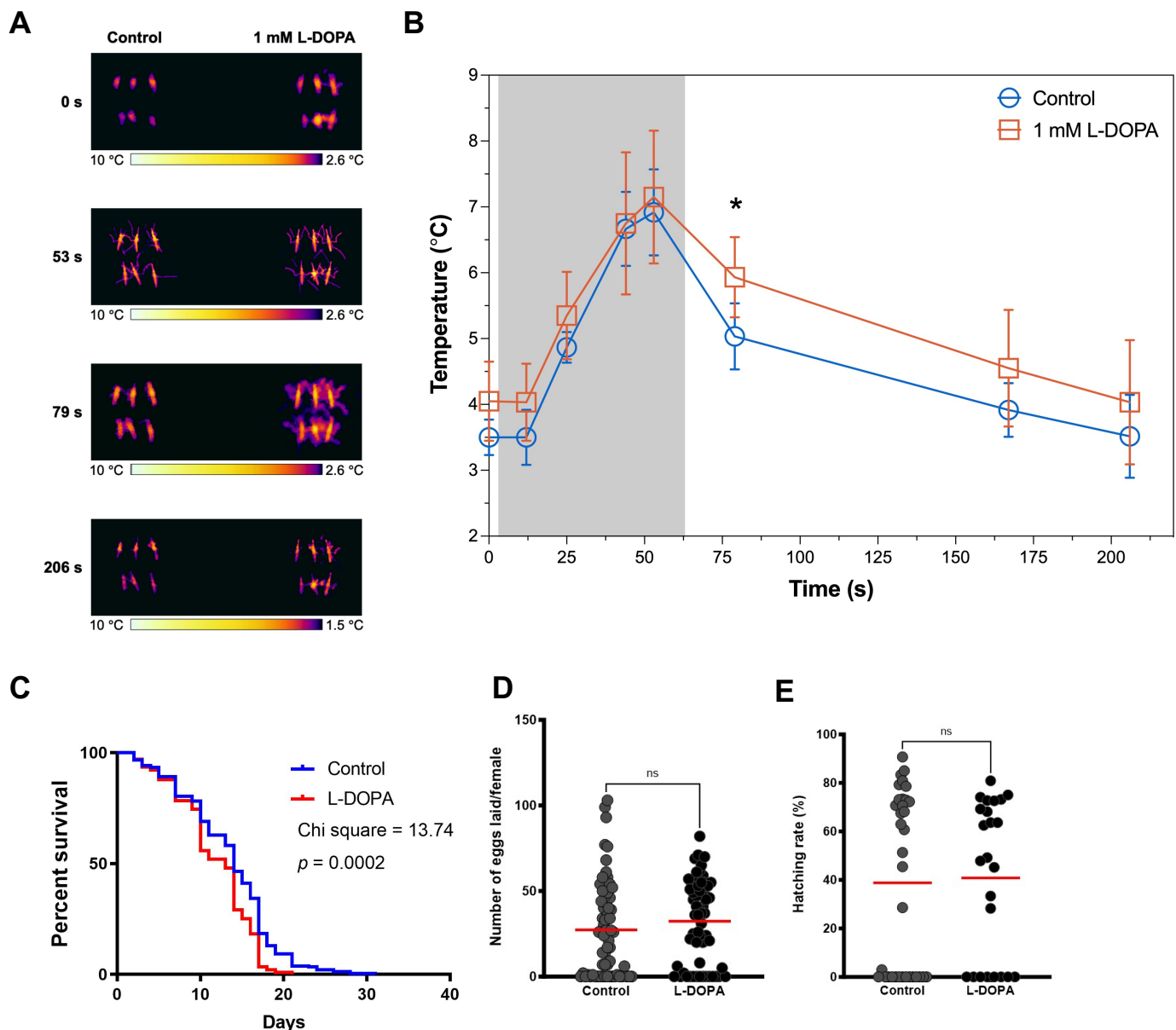
Fig. 8. Dietary L-DOPA darkening of cuticle increases heat-exposed mosquito temperatures following light exposure and decreases lifespan. A) *A. gambiae* female mosquitoes fed with a sugar meal supplemented with 1 mM L-DOPA for 8 d recorded ability to absorb augmented ability to capture heat eat. **B)** Exposure to a direct light source during 1 min (shadowed area) demonstrated that 1mM L-DOPA- fed mosquitoes (red squares) exhibited a warmer body temperature than sugar-fed control (blue circles). Post-irradiation when light is turned off (unshadow area), L-DOPA-fed mosquitoes (red squares) were distinctly hotter than sugar-fed controls (blue circles), starting to cool down but kept warmer than control The thermograph was obtained using the Teledyne FLIR E95 camera, and the temperature of each mosquito was extracted using the FLIR software, which provided the maximum, minimum, and average temperatures within a box selection for each mosquito. The maximum temperature for each mosquito was used to generate the graph, which represents the average (+/- Standard Deviation) of the six maximum temperatures corresponding to the two experimental groups (control sugar-fed and 1 mM L-DOPA-fed). Mann-Whitney test, p = 0.0173 **C)** Lifespan of mosquitoes maintained on 1.5% sugar with 1 mM L-DOPA was diminished in comparison to sugar-only fed mosquitoes. Data representative from 3 biological replicates. **D)** Number of eggs laid by female mosquitoes after feeding with a sugar meal supplemented with 1 mM L-DOPA during 4 d before a blood meal on mice. Mann-Whitney test, NS, not significant, p = 0.1987. Red lines denote mean. **E)** Hatching rate at 27 °C indicating average percentage of eggs giving rise to 1st and 2nd instar larvae. Mann-Whitney test, NS, not significant. p = 0.9390. Red lines denote mean.
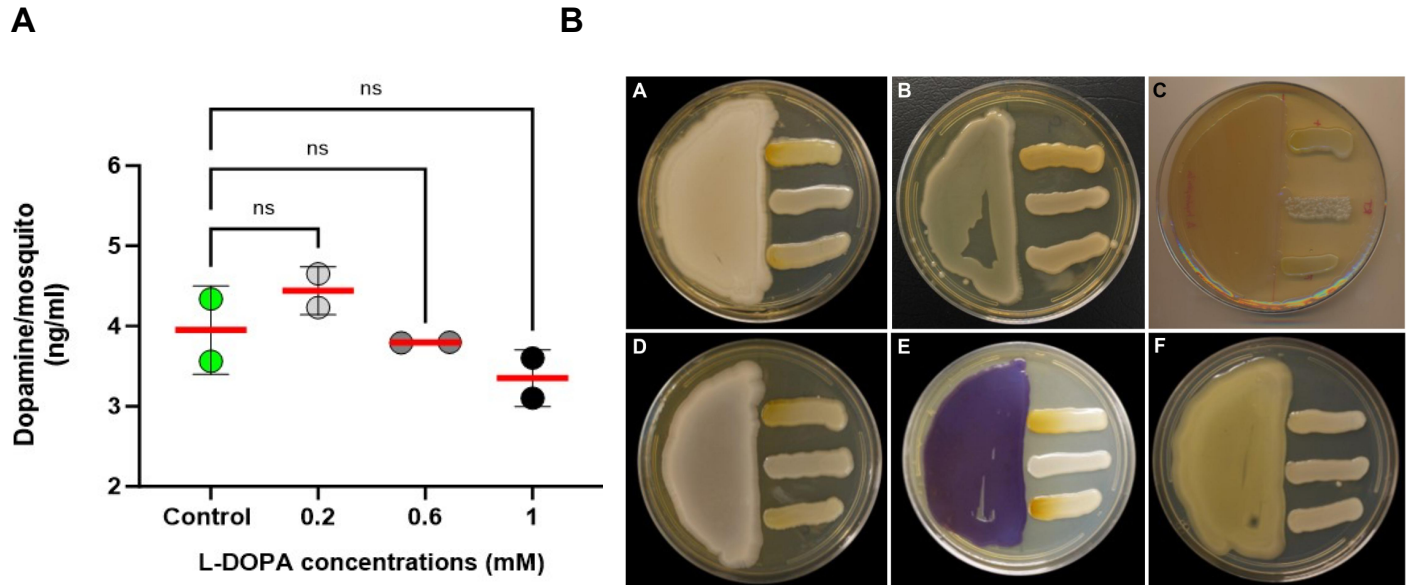
Fig. 9 Dietary L-DOPA metabolism and probing for dopaminergic bacteria amongst gut microbiota from field-caught mosquitoes.
A) Quantification of dopamine by HPLC from whole *Anopheles* mosquitoes post 4 d of dietary L-DOPA suggest a tight regulation of L-DOPA conversion into dopamine. Data corresponds to 2 independent biological replicates from 5-pooled mosquitoes per condition. A Two-way analysis of variance (ANOVA) with Sídák's multiple comparisons test showed no significant differences among and between groups. **B)** Plate confrontational assays showed induced fungal melanization due to melanin-precursors released by bacterial isolates. A) *Comamonas* sp.; B) *Enterococcus hormaechei*; C) *Aeromonas hydrophila*; D) *Serratia marcescens* E) *Chromobacterium subtsugae ΔvioS* F) *Enterococcus* sp. *Cryptococcus* strains (top: *C. gattii* WM179; middle: *C. neoformans* ΔLAC1; bottom: *C. neoformans* H99) were streaked perpendicular to bacterial isolates in SM plates. The plates were incubated at 30˚C for 5-7 days. Images are representative of 3 biological replicates.

Table 1. Detection of melanin precursors released by diverse bacterial species

Phylum	Class	Family	Strain	Source	Host	Location	C. neoformans induced melanization		Refs
							RT	30°C	
Firmicutes	*Bacilli*	*Bacillaceae*	*Bacillus* sp.	Midgut	Wild-caught *An. arabiensis*	Zambia, Africa	Negative	Negative	15
			Staphylococcus sp. A6	Midgut	Wild-caught *An. arabiensis*	Zambia, Africa	Negative	Negative	15
Proteobacteria	Betaproteobacteria	*Commonadaceae*	*Comamonas* sp.	Midgut	Wild-caught *An. arabiensis*	Zambia, Africa	Positive	Positive	15
		Neisseriaceae	*Chromobacerium subtsugae ΔvioS*	Soil/Water	None	New Jersey, USA	Positive	Positive	46,47
	Gammaproteobacteria	*Moraxellaceae*	*Acitenobacter* sp. PA6	Midgut	Wild-caught *An. arabiensis*	Zambia, Africa	Negative	Negative	15
		Aeromonadaceae	*Aeromonas hydrophila* S1	Midgut	Wild-caught *Ae aegypti*	Panama, Central America	Positive	Positive	45
		Enterobacteriaceae	*Enterobacter* sp.	Midgut	Wild-caught *An. arabiensis*	Zambia, Africa	Negative	Negative	15
			Enterobacter hormaechei PA	Midgut	Wild-caught *An. arabiensis*	Zambia, Africa	Negative	Negative	15
			Serratia marcescens N1.14	Midgut	Wild-caught *Ae aegypti*	Panama, Central America	Positive	Positive	45
			Pantoea sp.	Midgut	Wild-caught *An. arabiensis*	Zambia, Africa	Negative	Negative	15
			Proteus sp. PAI3	Midgut	Wild-caught *An. arabiensis*	Zambia, Africa	Negative	Negative	15
		Pseudomonadaceae	*Pseudomonas* sp.	Midgut	Wild-caught *An. arabiensis*	Zambia, Africa	Negative	Negative	15

RT, room temperature
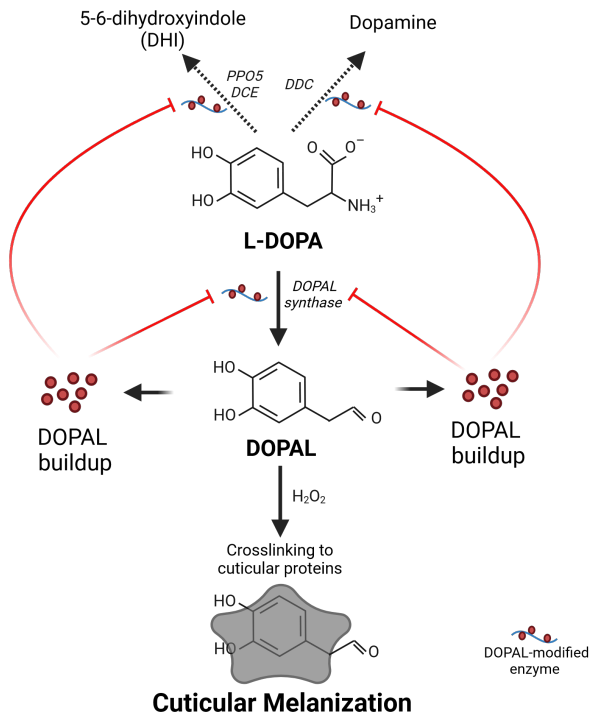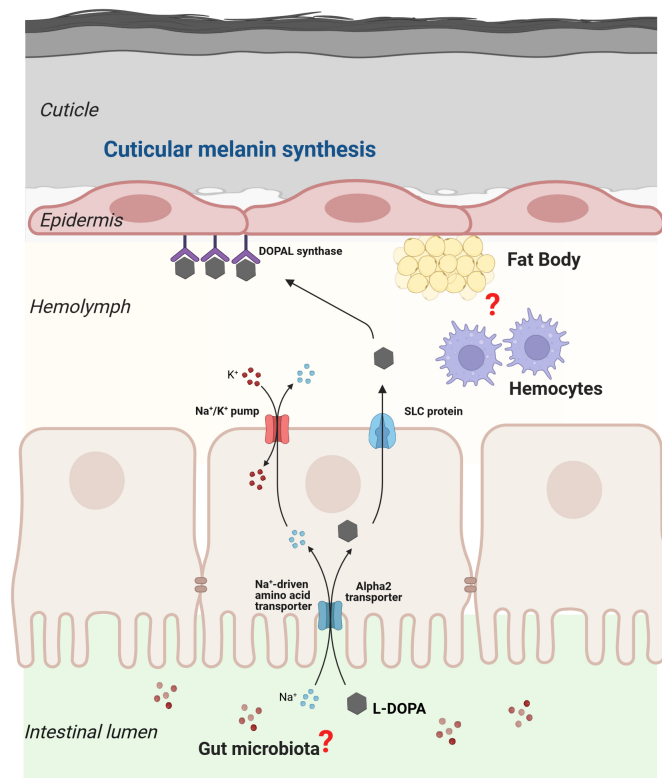
Fig. 10 Alternative pathway for L-DOPA incorporation to the melanin synthesis in mosquitoes. A) L-DOPA serves as a substrate for cuticular melanization via DOPAL synthase as a detoxification mechanism given a cellular redox environment that promotes L-DOPA antioxidant properties (neutral or acid pH) [60], therefore preventing its conversion to dopamine via a dopa decarboxylase. L-DOPA conversion into DOPAL leads into DOPAL buildup that promotes oligomerization and quinone adduct formation ("quinonization") inhibiting its own metabolism and the activity of other enzymes involved in the melanin biosynthesis such as dopa decarboxylase (DDC), phenoloxidase 5 (PPO5), and dopachrome conversion enzyme (DCE)[59] **B)** Model for dietary L-DOPA-mediated cuticular melanization proposes that *Anopheles gambiae* female mosquitoes use L-DOPA supplement in the sugar meal as a substrate for synthesizing cuticular melanin. L-DOPA is internalized into the midgut epithelium and exported to the hemolymph by sharing the same transporters with amino acids such as Na$^+$-driven amino acid transporter, alpha2 transporter, and/or SLC protein. Within regions of flexible cuticle, in the presence of DOPAL synthase, L-DOPA is turned into DOPAL and H$_2$O$_2$ promoting oxidation of DOPAL catechol ring that results in the formation of a melanized and protective flexible cuticle via crosslinking to cuticular proteins [57,58]. The contribution of gut microbiota as well as from hemocytes as key regulators of mosquito vectorial capacity and immunity, post a L-DOPA diet is under investigation. Figure created with Biorender.com